NASA TECHNICAL NOTE

NASA TN D-4032

NASA TN D-4032

ANALYSIS OF A BYPASS AIR CONTROL SYSTEM FOR A SUPERSONIC MIXED-COMPRESSION INLET

by Stuart C. Brown

Ames Research Center
Moffett Field, Calif.

NATIONAL AERONAUTICS AND SPACE ADMINISTRATION • WASHINGTON, D. C. • JUNE 1967

NASA TN D-4032

ANALYSIS OF A BYPASS AIR CONTROL SYSTEM FOR A SUPERSONIC MIXED-COMPRESSION INLET

By Stuart C. Brown

Ames Research Center
Moffett Field, Calif.

NATIONAL AERONAUTICS AND SPACE ADMINISTRATION

For sale by the Clearinghouse for Federal Scientific and Technical Information
Springfield, Virginia 22151 – CFSTI price $3.00

ANALYSIS OF A BYPASS AIR CONTROL SYSTEM FOR A SUPERSONIC MIXED-COMPRESSION INLET

By Stuart C. Brown

Ames Research Center

SUMMARY

An investigation was made of the control system parameters for an example bypass air flow control system for a simulated supersonic mixed-compression inlet. The engine inlet was simulated through use of an analog computer; the flow nonlinearities considered were obtained from wind-tunnel tests.

A criterion was developed for determining control system parameters, including effects of pressure signal location, for a given inlet. The criterion consisted of the determination of the maximum controllable engine disturbance rate subject to a time domain stability constraint. This constraint, based on the response of the controlled system to initial errors, was suitable for use with typical pressure signal nonlinearities including asymmetrical ones. Effects of variations in the stability constraint on the desired signal shape for a predetermined combination of linear system dynamics were obtained.

Effects of typical static pressure variations at different locations in the inlet when used as control signals were investigated. The departure from steady-state nonlinearity for the example signals downstream of the terminal shock wave tended to be in the opposite direction from the previously determined "desired" variation. The ability of an asymmetrical on-off system to control disturbances was also investigated. (A larger on-value was used to correct disturbances that tended to unstart the inlet.)

An investigation was also made with a linearized inlet representation of effects of different longitudinal signal locations and of variations in the dynamics of the associated control system components. For the control of engine disturbances, the pressure signal location near the aft end of the inlet was best. However, because of the influence of the remaining dynamics in the system, the improvement in the ability to control disturbances was only moderate.

The response of the linearized controlled inlet system to a statistically described longitudinal gust disturbance was calculated. The results showed that the control system requirements for the gust disturbance were less stringent than those for engine disturbances.

INTRODUCTION

Important aspects of the design of an airbreathing-engine inlet which operated above M = 2.2 are the variable geometry requirements and the associated control systems needed (refs. 1-6). For moderate supersonic speeds (below approximately M = 2.2), an external compression inlet is reasonably efficient; the flow is compressed through a series of oblique shock waves plus a normal shock wave outside the duct. At speeds greater than M = 2.2, the advantages of a mixed-compression inlet become significant. For this inlet, the final compression takes place within the duct and terminates by a normal shock wave just downstream of the inlet throat. The flow in this type of inlet is sensitive to operating conditions and hence requires accurate and rapid flow control. Moreover, a disturbance of sufficiently large magnitude will cause the normal shock to be expelled from the inlet, and the inlet to unstart. The concomitant flow fluctuations cause a mismatch with the engine flow demands, and a loss of thrust until the inlet geometry is varied in the proper sequence to restart the inlet.

For efficient stable operation of the inlet, two control systems are needed, one to control the inlet geometry and one to control the bypass flow. Geometry control is needed so that the inlet compression surfaces can be varied with supersonic flight conditions in order to obtain efficient inlet compression. Since flight conditions change fairly slowly, the response of the geometry control system can be slow. Bypass flow control is needed to match inlet airflow to engine requirements. The bypass control must have a fast response to correct any abrupt changes in engine flow and prevent an inlet unstart. Because of its fast response, it may also be used to correct for high frequency upstream disturbances, such as gusts. The bypass system can more readily control disturbances when the bypass flow is adjusted to position the terminal shock wave farther downstream from the throat. However, a compromise in this adjustment must generally be made since the farther the shock wave is positioned downstream of the throat, in order to decrease the likelihood of an inlet unstart, the greater is the loss in steady-state compression efficiency.

The selection of pressure signals adequate for the design of inlet bypass control systems is a problem because the signal must adequately describe changes in flow conditions due to disturbances over the full range of flight conditions. While intuitively it appears that locations near the aft end of the inlet provide the best signals to control engine disturbances, these locations have certain disadvantages. The signal gain is relatively low, so that the difference between the operating-point pressure and that at which unstart occurs is relatively small. In addition, the operating-point pressure signal required for different flight conditions must be known accurately. At more forward locations, the signals have greater pressure variations but may be more nonlinear.

In this report, attention will be directed to the synthesis of the bypass control system for a representative axially symmetric mixed-compression inlet. A suitable criterion will be determined for the evaluation of system

parameters including effects of control signal nonlinearities. Typical effects of pressure signals at different locations and the influence of several control system parameters on the ability of the system to control internal (engine) disturbances will be examined. Some results will also be presented on the effect of adding an on-off control signal to a continuous signal as well as the performance with only an asymmetrical on-off control. The use of this latter technique could simplify the control system. While the emphasis of the report is on the control of the engine disturbances, some preliminary results on effects of statistically described external gust disturbances on the inlet will also be presented.

The representation of the inlet dynamics incorporates wind-tunnel test results and includes pertinent nonlinear effects. The tests were conducted in the Ames 8- by 7-Foot Supersonic Wind Tunnel and a portion of these results was reported in reference 1. The computed results of the control system performance were obtained with an analog computer.

SYMBOLS

A_{bp}	area of bypass opening
M	Mach number
$\frac{m_d}{m_o}$	mass flow in duct just forward of bypass opening divided by inlet capture mass flow
N	average number of selected magnitude crossings with positive slope per unit time
N_o	average number of zero crossings with positive slope per unit time
p	static pressure
p_t	total pressure
RIAE	constraint on degree of stability; value of absolute error integral after first zero crossing divided by the value before the first zero crossing (see Selection of Criterion)
$RIAE_{dz}$	constraint on degree of stability for on-off system with dead zone
s	Laplace transform variable
T_t	total temperature
u_g	velocity of longitudinal gust
w	weight flow rate at a longitudinal station of the inlet

w_c corrected weight flow in inlet just ahead of bypass opening, $\frac{w\sqrt{T_t/T_{t_{std}}}}{p_t/p_{t_{std}}}$, percent increase from inlet unstart condition (percent supercritical)

w_{c_d} engine disturbance expressed as incremental corrected weight flow, percent supercritical

w_{c_e} incremental corrected weight flow error, actual minus operating point value, percent supercritical

$w_{c_e}(0)$ initial value of corrected weight flow error

x_s increment in shock wave position on center body from value at critical flow condition, positive in downstream direction

$\Delta(\ )$ increment of ( ) from value at operating point

ζ damping ratio

η_r ratio of total pressure at the aft end of the inlet to free-stream total pressure

σ_u rms of longitudinal gust velocity

σ_{x_s} rms of shock wave excursion about the mean value

τ time delay

Φ_u power spectrum of longitudinal gust

ω frequency

Subscripts

c controlled

d engine disturbance

m maximum value

op operating point; desired steady-state operating condition for bypass system

std standard or reference value

uc uncontrolled

∞ free-stream condition

$(\dot{\ })$ differentiation with respect to time

SYSTEM REPRESENTATION

A block diagram representing the inlet bypass flow control system to be analyzed is shown in figure 1. The purpose of the control system is to adjust the inlet airflow to a desired operating condition by diverting a portion of the flow through the bypass. A given command signal, which is a function of the flight condition and desired inlet operating condition, is sent to the controller. The controller also receives a signal pressure and divides it by a reference pressure to minimize effects on the signal of changes in flight conditions. This signal is compared with the command signal. Any resulting error causes a change in the bypass door opening. Thus there are changes in the amount of flow diverted through the bypass opening as well as in the signal pressure and in flow conditions throughout the subsonic portion of the inlet. The inlet flow is continuously corrected until the pressure error determined by the controller is nulled. For efficient operation of a mixed compression inlet, the inlet flow must be controlled within fairly precise limits, and in particular an error must not be sufficiently large to cause an inlet unstart. An error in the direction opposite to that which results in inlet unstart also must be limited to prevent excessive flow distortion and mismatch with the engine flow demands. However, this error can be of considerably greater magnitude than that in the inlet unstarting direction. Hence, an analysis must be made of the maximum errors which result with the controlled inlet for the expected disturbances to the inlet.

Inlet Representation and Disturbances

In this section, the form of the inlet representation for the subsonic portion of the started inlet and a brief description of the example inlet will be given. A description of the inlet disturbances to be used will also be included.

Inlet representation.- The general form used to represent the inlet, sketch (a), is an expansion of the inlet block shown in figure 1. Pertinent time histories, with the exception of the statistical averages obtained for the gust disturbance, were generated with an analog computer.

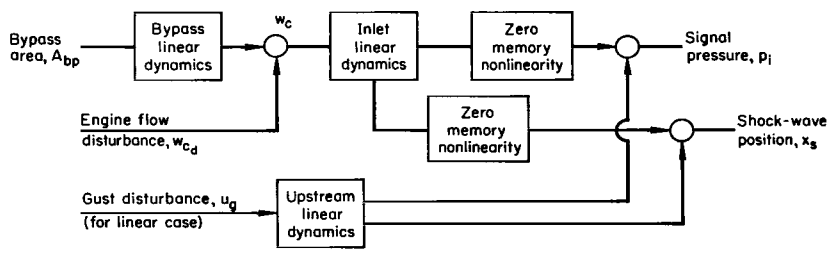

Sketch (a)

The disturbances to the inlet are indicated as well as the separation of the inlet representation into linear and nonlinear portions. Flow

disturbances from the engine and bypass opening are summed to form the perturbed flow in the inlet just forward of the bypass exit. The inlet linear dynamics block represents the dynamics between the flow at this aft location and at a more forward location selected for the control signal p_i and also the shock-wave position x_s. Except where needed as a control signal, the x_s term is used only to indicate when an inlet unstart occurs. A nonlinear function is included on the output side of the inlet linear dynamics. This arrangement follows from the fact that the principal flow losses and resulting nonlinearities occur in the forward portion of the inlet. In general, effects of both the dynamic terms and the nonlinearities become greater for the more forward control signal locations (up to the shock-wave position).

Corrected weight flow, w_c, was selected as a reference parameter to indicate average flow conditions at the longitudinal station just forward of the bypass opening. The parameter was expressed as percent increase from the critical value at which an inlet unstarts. Although pressure signals could have been computed without the intermediate determination of w_c, this parameter is useful for evaluating flow errors in the bypass region when the effects of pressure signals are compared for different locations and when the dynamic performance of other inlets is compared. Moreover, the parameter is used as an error quantity for the stability constraint in the determination of control system values subsequently described. Changes in corrected weight flow are proportional to changes in bypass area for the steady-state one-dimensional flow of a perfect fluid because of conservation of mass.

The bypass linear dynamics block in sketch (a) represents the flow changes, w_c, just forward of the bypass opening which result from bypass area, A_{bp}, changes. Two factors affect the bypass dynamics. First is the average rate at which flow changes are distributed through the inlet volume and second is the possible presence of restrictions on the flow after it leaves the bypass opening. For the range of flow changes investigated, a linear representation of the bypass dynamics is adequate.

Although the report is primarily concerned with effects of engine disturbances, some effects of an external longitudinal gust are also presented. The magnitudes of the disturbances investigated are sufficiently small that linear approximations are valid. The upstream linear dynamics block in sketch (a) represents the dynamics between a change in velocity immediately in front of the terminal shock wave and the subsequent shock-wave motion. Because only small changes are considered, the percentage change in this velocity is the same as the change in free-stream velocity.

Example inlet.- The numerical values to be used were obtained from wind-tunnel test results for a one-third scale axisymmetric inlet designed for mixed compression operation at $M = 3.0$ and with a boundary-layer bleed system near the throat (fig. 2). The inlet internal area distribution from the cowl lip to the bypass exit location is shown in figure 2(b). A volume aft of the inlet was included to simulate the effect of an engine on the inlet dynamics. This volume was about twice that between the throat and bypass opening and it extended about 1.6 meters beyond the bypass opening before exiting to the tunnel flow. Variations in the pertinent steady-state inlet flow parameters

with percent supercritical flow are shown in figure 3. The shock-wave position curve is shown as the distance downstream from the value for which the inlet unstarts. The pressure recovery curve indicates the compression efficiency of the inlet and has a direct effect on engine thrust and fuel consumption. The variation of the mass flow ratio is due to changes in throat bleed mass flow which also cause variations in aircraft drag.

For the bypass linear dynamics (sketch (a)), the following first-order transfer function was obtained by a linear curve fitting of the measured response of the pressure (near the bypass) to a sinusoidal bypass excitation.

$$\frac{w_c}{A_{bp}} = \frac{0.107}{1 + 0.012\ s}\ , \text{ percent/cm}^2$$

While the relationship between the corrected weight flow and the inlet static pressure distribution near the bypass exit was measured only for steady-state conditions, the same relationship between the two parameters was assumed to hold dynamically for the frequency range of interest (i.e., instantaneous values of static pressure were assumed to indicate instantaneous values of total pressure and temperature in determining the corrected weight flow. Note that since corrected flow is an intermediate quantity, any errors in its simulation do not affect the accuracy of the independently determined relationships between the inlet input and output quantities.

The inlet linear dynamics (sketch (a)) also were obtained from measured responses to sinusoidal variations in the bypass opening. The steady-state (zero memory) nonlinear function (f_i) between w_c and the pressure at a station (i), p_i, was determined. Then the measured frequency response between w_c and the function of p_i was matched to a linear dynamic form. For the example case, a time delay was used as follows

$$p_i(s) = f_i(w_c e^{-\tau_i s})$$

The time delay had a maximum value of 0.006 second for pressures near the throat and for the shock-wave position. This form was adequate for describing the example inlet dynamics for the measured frequency range up to 30 Hz. As previously mentioned, the principal nonlinearities in the flow occur near the throat of the inlet. (Signal nonlinearities will be shown in the Results and Discussion Section for particular locations and a fitted pressure representation will be compared with wind-tunnel results.)

Engine disturbances.- The engine, or internal, disturbances to the inlet are considered to be in the form of a corrected weight flow disturbance to the inlet flow (sketch (a)). In the performance criterion described in a subsequent section, the reference engine disturbance selected will be a ramp shape. This shape will be related to some predicted engine disturbances for a supersonic transport (SST) class engine.

Gust disturbances.- While most of the report is concerned with the control of engine disturbances, the determination of the response of the resulting system to an external statistically described gust will also be

presented. The gust disturbance is assumed to be only a change in the flow velocity. (An examination of steady-state flow conditions indicates that the gust direction which has the greatest tendency to unstart the inlet is a longitudinal gust which tends to decrease the air velocity relative to the aircraft.) Since measured flight data have substantiated that both longitudinal and vertical components of gusts have the same average magnitude for a given turbulence condition, results which have been obtained principally from vertical gust measurements will be used for longitudinal gust values.

The motions of the aircraft induced by longitudinal gusts would have small effects on inlet flow compared with the gust disturbance itself. Both the aircraft phugoid and short period modes are affected by longitudinal gusts. However, the phugoid mode is of sufficiently low frequency to have only a small effect for the frequency range of interest and the short period mode is principally vertical rather than horizontal motion. Hence, the effects of aircraft motions will be neglected in the representation of wind velocity changes relative to the inlet. An effect that may be important, but that is beyond the scope of this report, is the influence of aircraft motions on flow distortion near the inlet.

Values of the power spectral representation of longitudinal gusts were obtained through the use of references 7, 8, and 9. The gust data in reference 8 are principally for lower altitudes than those of interest for $M \approx 3$ cruise conditions. More recent measurements are included in reference 9. Since the results in the present report pertain to an approximately one-third size model, the scale of the turbulence selected for the full-scale gust power spectrum, 1000 meters, was reduced by a factor of 3. Hence, the time frequency scale for the power spectrum was also increased by a factor of 3. The results will be computed for a unit mean squared gust velocity $(\text{mps})^2$. Conversion to other mean square values can readily be made since the analysis is linear. The resulting constants for the form of the longitudinal gust power spectrum given in reference 7 are (for a unit mean square gust velocity and $M = 3$ cruise velocity)

$$\Phi_u = \frac{0.0703}{\pi[1 + (0.378\ \omega)^2]}, \quad \frac{(\text{mps})^2}{\text{rad/sec}}$$

ω in radians/sec. The power spectrum used is defined so that a symmetrical power spectrum of a quantity is related to its mean square value by the equation

$$\sigma^2 = \int_0^\infty \Phi(\omega)\, d\omega$$

Determination of inlet unstarts due to gust disturbances.- Transfer functions are needed to relate changes in free-stream longitudinal velocity to changes in terminal shock-wave position and to changes in the pressure signal used for the closed loop system (sketch (a)). For this linearized case, a pressure signal at a point close to the shock wave, which corresponds to a signal proportional to the shock-wave position, was used for control. A previously computed transfer function, determined for a similar full-scale

axisymmetric inlet operating at M = 3.0, was modified to provide an estimate for the one-third scale model used in the present report. This computed transfer function was determined through use of a method of characteristics digital computer program developed in a previous portion of the study described in reference 1. The modified transfer function is

$$\frac{\Delta x_{s_{uc}}}{u_g} = \frac{0.103}{\frac{s}{300} + 1} \frac{\frac{s}{19.3} + 1}{\frac{s^2}{148{,}000} + \frac{s}{246} + 1}, \qquad \text{cm/mps}$$

In modifying the transfer function to represent that for the model, all frequency terms were increased by a factor of 3 and the gain was reduced by a factor of 3. While some differences in geometry exist between the two inlets, the modified transfer function is felt to be at least a first approximation to the desired one.

A transfer function is needed to relate the terminal shock-wave displacement for the controlled system, Δx_{s_c}, to an external disturbance; this disturbance was expressed in the form of a shock-wave displacement for the uncontrolled case $\Delta x_{s_{uc}}$. Constants needed for the transfer function for the controlled system were determined, from the criterion to be discussed in the following section, by means of the analog computer.

From the preceding relations, the power spectra for shock-wave excursions due to gust disturbances can be expressed for the uncontrolled case as

$$\Phi_{x_s}(\omega) = \frac{\Delta x_{s_{uc}}(j\omega)}{u_g} \frac{\Delta x_{s_{uc}}(-j\omega)}{u_g} \Phi_u(\omega) \sigma_u^2$$

and for the controlled case

$$\Phi_{x_s}(\omega) = \left[\frac{\Delta x_{s_c}}{\Delta x_{s_{uc}}}(j\omega) \frac{\Delta x_{s_c}}{\Delta x_{s_{uc}}}(-j\omega)\right]\left[\frac{\Delta x_{s_{uc}}}{u_g}(j\omega)\right]\left[\frac{\Delta x_{s_{uc}}}{u_g}(-j\omega)\right] \Phi_u(\omega) \sigma_u^2$$

The resulting mean square value of the shock-wave excursion was determined by a numerical integration of the equation

$$\sigma_{x_s}^2 = \int_0^\infty \Phi_{x_s}(\omega)\, d\omega$$

The mean square shock-wave excursion, $\sigma_{x_s}^2$, is proportional to the mean square turbulence level, σ_u^2, selected.

The average number of inlet unstarts per unit time for a given operating point expressed in terms of the shock-wave position, $x_{s_{op}}$, and a selected turbulence level, σ_u, was obtained by a numerical integration of the following equation (ref. 7).

$$N = N_o \exp(-x_{s_{op}}^2/2\sigma_{x_s}^2)$$

where

$$N_o = \frac{1}{2\pi\sigma_{x_s}} \left(\int_o^\infty \omega^2 \Phi_{x_s}(\omega)\, d\omega \right)^{1/2}$$

Although used for a somewhat different purpose in reference 7, the equation is also applicable to the present case since it indicates the average number of positive slope crossings of a certain level per unit time for a gaussian distributed random process.

Controller and Actuator

The remaining components of the bypass control system shown in figure 1 are the controller and servo actuator. Example numerical values to be used for these components were obtained through use of bench test results reported in reference 1. The controller is a special purpose device which receives a signal pressure input, divides it by a reference pressure, and compares it with a desired value for the particular flight condition. Since only one flight condition will be investigated, only the generation of an error signal by the controller was simulated. While nonlinearities in the controller can be important, only second-order linear dynamics were used for this report. The nominal values simulated were a natural frequency of 35 Hz and a damping ratio of 0.8 as shown by the following transfer function with a normalized gain.

$$\frac{\text{Output}}{\text{Input}} = \frac{1}{1 + \frac{2(0.8)s}{220} + \left(\frac{s}{220}\right)^2}$$

The servo valve and actuator are relatively conventional hydraulic components as far as their operating characteristics are concerned. While their nonlinear variations should be considered for a complete simulation, they will not be included in this report. The servo-valve dynamics were represented by a linear second-order term and the actuator by a single integration. The nominal servo-valve dynamics used were a natural frequency of 28 Hz and a damping ratio of 0.7. Thus the servo valve and actuator dynamics were represented by the following equation.

$$\frac{\text{Output}}{\text{Input}} = \frac{1}{s\left[1 + \frac{2(0.7)s}{176} + \left(\frac{s}{176}\right)^2\right]}$$

Note that the actuator performs as an integrating element so that a step input to the servo valve results in a steady-state constant velocity of the actuator. While a fairly wide range of servo-valve dynamics is feasible, a somewhat conservative value was used for this case. Some effects of variations in the

servo-valve and controller frequencies will subsequently be shown. While neglected for this case, the dynamics of the hydraulic transmission lines sometimes need to be included.

Control Signal Modifications

Two discontinuous modifications of the control signal were also investigated. One was an on-off control which consisted of a different magnitude of the on signal for the error in each direction and a dead zone near the operating point value. The use of this form of signal would result in potential simplifications in the pressure sensor, controller, and/or servo-valve. Since the control of errors due to disturbances which tend to unstart the inlet is more important than the control of those which act in the opposite direction, the magnitude of the on signal to correct errors due to an unstart tending disturbance was made greater. The use of a sufficiently large signal to correct errors in one direction makes it possible to minimize the errors due to disturbances in this direction. A limit cycle in the absence of disturbances was prevented by use of a dead zone and a sufficiently small corrective signal for errors in the opposite direction. This improvement in the control of errors in one direction is done, of course, at the expense of allowing larger flow errors in the opposite direction. Criteria used to select the on-off parameters will be given in the following section. The on-off signal was simulated between the controller and servo as shown in sketch (b).

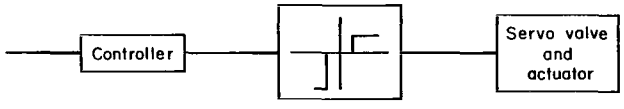

Sketch (b)

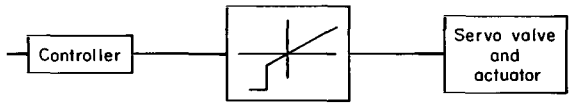

Sketch (c)

The second discontinuous modification investigated was the addition of a maximum on signal in one direction only when the signal error exceeded a certain value. This type of signal would provide greater control power to counteract disturbances in the unstart direction, but would not affect the stability near equilibrium. This nonlinearity, at the same location as the previous one, is shown in sketch (c). The addition of this signal would be particularly useful when the gain of the signal pressure decreased as the inlet critical flow condition was approached.

SELECTION OF CRITERION

The primary purpose of the bypass control system is to minimize the maximum flow errors due to flow disturbances to the inlet. This need to make the system as impervious to disturbances as possible leads to the use of a high gain system with its attendant stability problems. Hence, the selection of a criterion for evaluating the system includes the selection of a representative maximum disturbance to be controlled as well as some constraint on the transient behavior of the system which relates to its degree of stability.

Moreover, a constraint is needed which is useful with nonlinear signals and particularly with asymmetrical nonlinear signals. In addition, disturbances which tend to cause an inlet unstart are of greater concern than those in the opposite direction, so that a criterion for which asymmetrical properties can be deliberately selected is desirable. The criterion can be used to adjust control system parameters of a selected form to control the largest possible disturbance while still satisfying the requirements of the stability constraint. Besides being used for comparing the performance for the same inlet with different control signals, the criterion can be used to compare the closed-loop performance of different inlets.

Representative Disturbances

A representative disturbance shape will be selected for which the control system parameters will be adjusted to reduce the maximum flow error. The inlet is subject to both external disturbances, such as passing shock waves due to other supersonic aircraft and gusts, and internal disturbances due to the engine. Previous estimates of the effects of such disturbances on inlets indicate that the disturbances of larger magnitude were caused by the engine. Although the frequency spectrum for the external disturbances tended to have a somewhat wider bandwidth, the most critical was felt to be an engine disturbance. However, preliminary results for an external gust disturbance will also be given. The reference engine disturbance shape selected was a decreasing corrected weight flow ramp which begins with the flow at a steady-state condition. This direction of the disturbance tends to unstart the inlet. Some estimated example engine flow disturbances are shown in figure 4 (ref. 1). These disturbances represent flow changes at the bypass station for the uncontrolled inlet. The time in which the full scale disturbances occur has been reduced by a factor of 3 to be compatible with the one-third scale inlet dynamics. The maximum disturbance rate occurs initially for each case. Of the three cases shown, the turbofan afterburner hard light case is the most critical as far as inlet unstart is concerned with a maximum disturbance rate of about -185 percent per second. While for the complete engine-inlet system it may be desirable to modify the engine controls and signals in order to reduce the effect of engine disturbances on the inlet, the present report will be concerned only with selecting the inlet parameters to control the selected form of disturbance.

The criterion selected is to determine, for a given operating point, the maximum rate of decrease of airflow which can be controlled without causing an inlet unstart. A degree of stability constraint on transient behavior will be presented in the next section. A typical time history of normal shock-wave position for a maximum controllable ramp disturbance starting from equilibrium initial conditions is shown in sketch (d). For a relatively high control system gain, the shock wave position transient will have some overshoot, followed by a steady value dependent on the magnitude of the disturbance rate since an integration is included in the control loop. The maximum error, shown in sketch (d), for the response to a constant ramp disturbance from

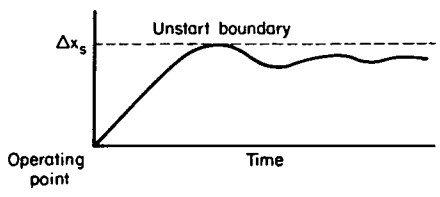

Sketch (d)

equilibrium conditions will be indicative of the maximum errors due to disturbances such as those shown in figure 4 for relatively high gain systems. Hence the maximum controllable rate is the principal disturbance parameter for these systems as indicated by the high gain curve in sketch (e). The unstart boundaries in sketch (e) are combinations of disturbance rate and maximum amplitude for which an inlet unstart would occur without any limiting of the bypass opening. The vertical boundary represents the uncontrolled case. As the gain is increased for the controlled case, the controllable region under the curve is increased. For a system with relatively low gain, the steady-state error due to a ramp disturbance is approached asymptotically without overshoot so that the duration of the ramp modifies a larger portion of the boundary as shown by the low gain curve in sketch (e). Since most of the results will be concerned with performance for the high gain cases, only the limitations on maximum disturbance rates, as shown by the right-hand portions of the curves, will be presented.

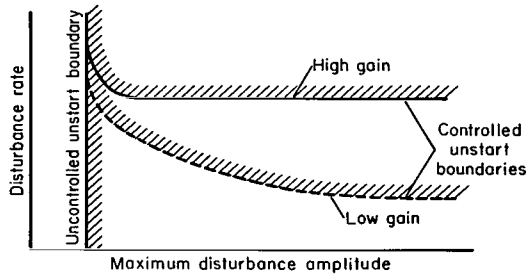

Sketch (e)

Stability Constraint for the Continuous System

The need for a control system that will keep flow variations due to disturbances as small as possible leads to the use of a high gain system with its attendant stability problems. It was desired to select a constraint on stability of the motion with respect to the operating point which was suitable for the closed loop control system considered. The system response has zero final error due to a step change in the command signal. For the linear case, the system is characterized by a pair of dominant roots due to the inlet bypass and actuator dynamics, but which are influenced by the controller and servo-valve dynamics as well as the inlet dynamics. A time domain constraint which could be used with moderate departures from linearity in the system and which was suitable for computer analysis was desired

The stability-constraint selected was a bound on the overshoot response of the system to an initial flow error without a disturbance present. This bound is the value of the time integral of the absolute error after the first zero crossing divided by the integral before the first zero crossing. Hence, a measure of the ability of the system to correct to and maintain a desired value is obtained. The two integrals are shown by the two shaded areas in sketch (f).

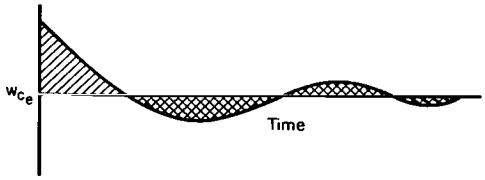

Sketch (f)

The transient error quantity selected for the constraint was the inlet corrected weight flow just forward of the bypass exit. The flow at this station was felt to be more indicative of the corrective bypass control applied than flow indications at other stations such as the shock-wave position near the throat. The initial error simulated, starting from an initial steady-state flow condition,

was a step signal to the controller to return the inlet flow to a desired operating point condition. The degree of stability constraint for which this "ratio of the integral of the absolute errors" is used will be designated RIAE. This constraint is seen to be similar to a maximum overshoot constraint. However, the RIAE constraint is felt to have an advantage over maximum overshoot constraint in that it will influence the design of the system if an additional higher frequency, lightly damped oscillation is also present in the transient. Note that the RIAE constraint is useful for either linear or nonlinear systems which result in zero final error. A modified form of the constraint can be used for systems with dead zones or hysteresis nonlinearities by the use of integrals of the error quantity outside the hysteresis or dead zone.

For a nonlinear system, the value of the integral ratio will vary with the magnitude of the initial error, although for a linear system it is independent of this quantity. Hence, for the nonlinear cases, the value of the integral must be evaluated for the range of initial conditions of interest. On the other hand, it will be advantageous to purposely vary the desired value of the RIAE constraint with initial error to meet particular control requirements. Since requirements for control for the present case depend on the direction of the disturbance, it is desirable to specify an asymmetrical variation. In order to obtain an increase in the maximum controllable disturbance ramp which tends to unstart the inlet, but still maintain the degree of stability near the operating point, the stability constraint requirements were relaxed for initial errors in the unstart direction in the manner shown in sketch (g). The value of the RIAE constraint increases linearly with magnitude of the negative initial error from that at the operating point flow condition to a maximum at the inlet unstart condition. For positive initial flow errors, the constraint remains constant. The effect of using this form of the constraint is seen to be that a larger corrective signal can be applied for the larger negative flow errors, while a more stable behavior for errors near the operating point and for positive flow error is maintained. The effect of different maximum values of the constraint on the ability to control disturbances and the resulting desired signal shape for the example inlet will be shown in a later section. The range of initial errors selected to satisfy the constraint for the increased corrected air flow was the same as that for the decreased corrected flow. For an actual case, the increased flow limit would be determined by inlet flow distortion and inlet-engine mismatch considerations. For the results which will be presented, a value of RIAE = 0.1 was selected for initial positive corrected flow errors.

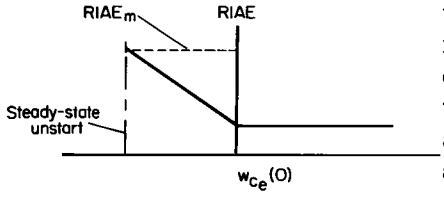

Sketch (g)

A closed form result for the effect of the constraint can be obtained for a simplified linear case. If the controller, servo valve, and inlet dynamics are neglected, and the bypass dynamics are represented by a first order term, then the order of the system is reduced to second order. The damping ratio of the system can be expressed as a function of the open loop gain and then the transient response for the selected initial condition is a function of the damping ratio. An expression for the RIAE integral ratio constraint can therefore be derived as the following function of damping ratio:

$$RIAE = \frac{\coth(\zeta\pi/2\sqrt{1-\zeta^2})}{1 + 2\zeta \exp[(\zeta/\sqrt{1-\zeta^2})(\pi - \cos^{-1}\zeta)]}$$

For the selected RIAE constraint of 0.1, the loop gain is restricted to a value such that the system damping ratio ≥ 0.67.

Stability Constraint for On-Off System

The RIAE constraint previously described cannot be used when the final error for a transient is different from zero. For the on-off system described in the System Representation section, a modification of the stability constraint is needed since the final error is not zero because of the dead zone. Moreover, a different constraint for the signal level in each direction will be selected; the one to correct negative initial flow errors would be less stringent. The initial flow error range was selected to be the same as for the continuous case. For the on signal which corrects positive initial flow errors, the constraint selected was such that zero overshoot should occur for the maximum positive initial error of interest (see solid curve in sketch (h)). This restriction provides a margin for the prevention of a limit cycle with no disturbance present since the opposite dead zone boundary is not crossed even for large initial positive errors. The signal which corrects negative flow errors was restricted so that the ratio of the integrals of errors outside the dead zone was within a selected value, $RIAE_{dz}$, for the most negative initial error of interest (see areas under dotted curve in sketch (h)). Thus, for a selected $RIAE_{dz}$ constraint, a parameter search was made with the analog computer for the combination of positive and negative signal levels and symmetrical dead zone which yielded the largest ramp disturbance (tending to unstart the inlet) which could be controlled.

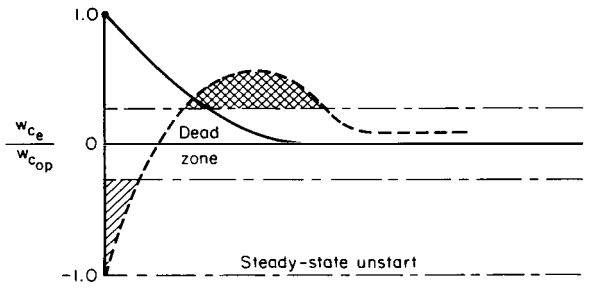

Sketch (h)

RESULTS AND DISCUSSION

The results, obtained with an analog computer, will be presented as follows: (a) A brief comparison will be made between calculated inlet dynamics and wind-tunnel test results to demonstrate the adequacy of the inlet representation. (b) The effect of several variations in the previously discussed RIAE stability constraint on the maximum engine disturbance rate which can be controlled will be given for the example inlet and nominal control system dynamics. (c) The optimum signal pressure variation required to achieve the results noted in item (b) will be presented. (d) The control system performance, using a fixed RIAE stability constraint, will be compared for several different locations of the control signal. (e) Effects of deliberate

control signal simplifications including an on-off control will also be presented. (f) For the linearized case, some effects of variations in the inlet and system component dynamics and of the use of lead on the ability to control engine disturbances will be presented. (g) Some preliminary results of the influence of statistically described gusts on the inlet operation will also be presented.

A brief discussion of the example inlet and the numerical values used are given in the System Representation section along with nominal values of the controller and servo dynamics.

Comparison of Simulated Inlet Dynamics With Experiment

A brief indication of the adequacy of the form used to represent the inlet response to a bypass flow input as described in the Inlet Representation section is shown figure 5. The response of static pressure 1.3 cm aft of the geometric throat on the centerbody to a particular sinusoidal bypass area amplitude is shown. The function, p/p_{t_∞} vs. w_c, is the zero memory nonlinearity for the inlet representation in sketch (a). Since the normal shock wave moves past this station for the flow disturbance range selected, the static pressure varies only for the portion of time that the shock wave is upstream of the pressure orifice. The measured and computed wave forms have been centered relative to each other in order to facilitate shape comparisons. The phase differences as determined from peak values are also shown. The computed results give good agreement with the measured results for the frequency range shown. It should be noted that with this form of representation, the computed wave forms are symmetrical about each peak. For stations farther downstream for which both positive and negative peaks occur, the computed positive and negative peaks are one-half of the excitation period apart as in the linear case.

Effect of Variations in Stability Constraint

As discussed in the Selection of Criterion section, it is desirable to relax the degree of stability constraint for large flow errors which tend to unstart the inlet (sketch (g)) so that larger disturbances in this direction can be controlled. The effect of changes in slope of the previously discussed linear variation in the constraint with initial flow error and the corresponding $RIAE_m$ is shown in figure 6. Both the maximum disturbance which can be controlled and the nonlinear signal shape for a given constraint variation are shown (figs. 6(a) and 6(b)). The inlet linear dynamics for a pressure sensor near the shock-wave position ($\tau = 0.006$ sec) were used. The only nonlinearity selected was the variation in pressure signal with inlet flow condition.

Since the stability constraint varies with initial flow errors in only one direction, the corresponding signal nonlinearity occurs essentially in only one direction (fig. 6(b)). The constraint is more stringent for the small negative initial errors than it is for the larger negative ones. Hence, the desired signal shape was obtained on the computer by determining the values for small initial negative flow errors and then increasing the initial

error range until the signal for the entire flow range of interest was obtained. The nonlinear curve in figure 6(b) is shown relative to a linear signal. This signal has been normalized such that a unit steady-state value would result in an inlet unstart. For the selected form of constraint variation and a given set of system dynamics, the resulting signal shape for the deviation from linearity was the same for the different values of $RIAE_m$. Hence, once this curve shape is determined, only the maximum values of the signal need to be given as shown in figure 6(a). For the example dynamics, an $x^{1.75}$ power curve matched the desired curve shape quite well and is shown in figure 6(a) for $RIAE_m = 1.5$. Furthermore, it follows that since the curve shape is independent of $RIAE_m$, the maximum signal can be expressed as the function of $RIAE_m$ shown in figure 6(a). A determination of the desired results with a simpler square power shape was also investigated for the range of $RIAE_m$ of interest. As indicated by the circled point on figure 6(a) for the maximum value of $RIAE_m$, the performance is not very sensitive for the example inlet to the difference between the $x^{1.75}$ and x^2 power curves. The addition of a cubic term was also investigated but the effect was too small to be shown on the figure. The effects of moderate variations in dynamics (for a fixed $RIAE_m$) on the desired curve shape were also investigated. To a first approximation, these differences could be accounted for primarily by a change in the maximum signal with the same signal shape rather than changes in the entire signal shape.

An improvement in the ability to control disturbances over the linear case ($RIAE_m = 0.1$) is seen to occur as the $RIAE_m$ constraint is relaxed. However, a point of diminishing returns is reached for the larger values of $RIAE_m$.

Some typical time histories are shown in figure 6(c). The resultant asymmetry in the nonlinear response is apparent from the two initial condition cases. While the response to the ramp disturbance becomes rather oscillatory, only the initial portions of the time histories up to the time that the first peaks occur are of interest.

As was previously discussed, the RIAE constraint used is similar to a maximum overshoot constraint but is useful for a wider class of systems. This improvement occurs because the RIAE integration allows an averaging effect and also is sensitive to any lightly damped higher frequency motions. The two constraints were compared briefly to determine the difference in optimum signal shape for a linear variation in the constraint with initial error. The best signal shape for the maximum overshoot constraint was found to vary near $x^{1.9}$ power as contrasted for the RIAE variation of $x^{1.75}$ power for the same system dynamics. For a selected maximum signal, the effect of this difference in signal shape on the maximum controllable ramp disturbance is very small for the example case.

To indicate the ability of the system to control a disturbance different from that used in the design, the effect of a sinusoidal engine flow disturbance is shown in figure 7. Two linear cases are shown for which the RIAE constraint is constant for the range of initial conditions. The RIAE = 0.1 value is selected to give good damping properties, while the RIAE = 1.5 value

is an example in which the stability constraint is relaxed so that the gain can be increased to reduce errors due to low frequency disturbances. The optimum nonlinear case is the same as that shown in the previous figure with $RIAE_m = 1.5$. For this case, the amplitude of the disturbance input for most of the frequency range was that which would just cause the inlet to unstart for the uncontrolled case. In the frequency range for which the negative error for the controlled case exceeded the uncontrolled one, the disturbance amplitude was reduced so that the inlet flow would just reach the unstart condition. Both negative and positive maximum deviations for the same input amplitude are shown.

The comparison from figure 7 shows that, for the linear case, the use of the RIAE = 0.1 constraint causes only a moderate amount of overshoot in the higher frequency range. The change to RIAE = 1.5 constraint permits an increased gain. While this change allows an improvement in the response at the lower frequencies, the response is worse at the higher frequencies near the natural frequency of the closed-loop system and is a consequence of the underdamped system. The flow errors in the direction of inlet unstart (maximum negative error) are seen to be less for nonlinear $RIAE_m = 1.5$ than for linear RIAE = 0.1 for the entire frequency range shown. This improvement occurs at the expense of greater flow errors in the opposite direction, for which the inlet flow requirements are more tolerant. The response for the nonlinear case is seen to be improved even at the higher frequencies. This improvement is a consequence of the combination of the asymmetrical nonlinearity and the actuator which is represented as an integrating element. For a periodic flow condition to occur, the average signal for the portion of the loop from the nonlinearity to the integrating element (from output of the inlet to input of the actuator) must be zero. The portion of the loop from the integration to the nonlinearity, which includes the corrected airflow quantity (sketch (a)), will have a steady-state component as well as a periodic one. The sign of this steady-state component depends upon the direction of the asymmetry of the nonlinearity.

Effect of Example Control Signals on Performance

In this section, the effect on bypass control system performance of several different static pressure control signals obtained from measured wind-tunnel results will be examined. The effects of these signals will be compared by means of the previously described criterion of the maximum controllable engine disturbance rate subject to the stability constraint.

A centerbody static-pressure signal near the normal shock wave is evaluated in figure 8. The steady-state variation of the signal with corrected flow is shown in figure 8(b). The indicated variations in signal gain are largely associated with changes in shock-wave location. Near the critical flow condition, the signal has a relatively low gain, but as w_c increases and the shock wave moves farther aft toward the signal location, the signal gain increases until the signal limits. The limiting indicates that the shock wave is downstream of the signal location. While this general behavior usually occurs near the normal shock wave, other cases can be considerably different, of course, because of factors such as proximity to a boundary-layer bleed

and the particular shock-wave pattern. Note that this variation in magnitude of signal gain with inlet airflow is the opposite from the desired variation shown in figure 6(b).

The consequence of this variation in signal gain on the ability to control a ramp disturbance is shown in figure 8 for a range of operating points expressed as the corrected weight flow parameter. The corresponding effects of operating point changes on pressure recovery and bleed flow can be obtained from figure 3. The particular RIAE constraint variation used is indicated in figure 8(a). In obtaining the example signal curve in figure 8(a), the loop gain was adjusted for each operating point to the maximum value for which the stability constraint was still satisfied. The optimum signal curve is that which would be obtained if the same signal shape shown in figure 6 were used relative to each operating point. While the same nonlinear variation with different operating points could not actually be achieved, of course, the curve is useful as a reference. Thus, the maximum controllable negative disturbance for the optimum signal has a linear variation with operating point as does the linear signal.

The performance resulting from the example signal is seen to be considerably reduced from the linear and optimum signals at the larger corrected flow operating points. This reduction is a consequence of adjusting the loop gain to meet the stability requirements for flow errors greater than the operating point value and for which the signal gain is relatively high. For flow errors less than the operating point value, the signal gain and, hence, the effectiveness of the control are reduced. Furthermore, since the use of the larger airflow operating points is accompanied by a reduction in steady-state pressure recovery, it is desirable, of course, to minimize this trend. Note that relaxing the RIAE constraint for a decreased airflow initial condition does not improve performance for this form of signal in which the magnitude of the signal gain increases with inlet airflow because the loop gain parameter is determined by the increased airflow initial conditions.

A comparison of the calculated controllable disturbance rates for the example signal (fig. 8) with the estimated engine disturbances (fig. 4) is of interest. The afterburner hard light with the -185 percent per second maximum disturbance rate is too large to be controlled without inlet unstart for the example signal and stability constraint selected. Even for the linear or optimum curves, the operating point value of airflow would have to be so large that the loss in steady-state pressure recovery would be significant (fig. 3). On the other hand, it is seen that the throttle advance disturbance (with an initial rate of about -40 percent/sec) can be controlled through use of the example pressure signal for an operating point with only a moderate loss in pressure recovery.

As was previously mentioned, the response of the control systems of interest is sufficiently fast that the maximum disturbance error generally occurs before the maximum value of the disturbance occurs. For instance, for the disturbances shown in figure 4, the maximum values in the negative direction occur in about 0.125 second while the transient response errors for the optimum and linear signals reach a maximum in less than this interval. However, for the example signal, the transient response to a negative ramp

disturbance decreases as the operating point is increased since the effective gain as the critical flow condition is approached is decreased (fig. 8(c)). A rise time to 90 percent of the final flow error of 0.125 second for the maximum ramp disturbance occurs for $w_{c_{op}}$ = 5.1 percent. Hence, for operating points appreciably greater than this value, the bypass control becomes less effective for this maximum disturbance frequency range of interest which is determined from the peak value in 0.125 second. Thus, the maximum disturbance amplitude for the uncontrolled case (as determined by the operating point) would become a more dominant parameter in determining the controllability of the disturbance.

The response in the negative flow error direction of the closed-loop system with the example pressure signal to a sinusoidal engine disturbance is shown in figure 9. Disturbance amplitudes were selected in the same manner as those for the results shown in figure 7. A sufficiently large operating point ($w_{c_{op}}$ = 7.5 percent) was selected so that nonlinear signal effects could be illustrated. The solid curve represents the case with the control gain adjusted for the $RIAE_m$ = 1.5 constraint and the selected operating point. The dotted curve indicates the effects of an increased control system gain. This increased gain is approximately the same as the increase in open-loop gain, for the portion of the control loop excluding the pressure signal, which was determined for the system with only slightly supercritical flow conditions. For these conditions the pressure signal gain was at its lowest value.

The comparison of the two curves is qualitatively similar to that expected for the gain variation for a linear signal. With the lower gain, the control is not as effective at the low frequencies, but no severe overshoot problem is encountered at the higher frequencies. The high gain case does indicate considerable overshoot which is characteristic of a lightly damped system. Note that even in the highest frequency range shown, the flow error for the controlled case is somewhat higher than that of the (unity) uncontrolled case. Again this difference is a consequence of the asymmetrical pressure signal as was noted for the optimum signal case shown in figure 7. For the example signal, the magnitude of the gain variation with airflow (fig. 8(b)) is in the opposite direction from that of the optimum signal (fig. 6(b)). Hence, the difference between the controlled maximum negative errors and uncontrolled errors at the higher frequencies is of opposite sign for the two cases (figs. 9 and 7).

One way to improve the response of a system with poor signal characteristics, such as that for the larger operating point values shown in figure 8, would be to add a second pressure source so that the summed signal would have the desired variation. A simplification of this approach is of interest in which a maximum "on" signal is sent to the servo-valve when a certain threshold pressure is exceeded due to a disturbance which tends to unstart the inlet. This threshold pressure signal could be obtained from either the same pressure source or a second one intended to give better accuracy near the on-signal threshold. For the case shown, the dynamics for the on-signal are the same as those for the example signal. The magnitude and threshold of this semi-on-off signal were selected for each operating point by means of the previously used RIAE constraint variation indicated in figure 8(a). Further

details concerning the simulation of the signal were given in the System Representation section. The addition of the semi-on-off signal is seen to result in a considerable improvement in performance over the example signal only (fig. 8). While performance could equal the optimum signal curve if a particular nonlinear function of the signal were generated by the controller (for flow conditions less than signal saturation), the improvement from the semi-on-off case would not be significant for this example.

The performance with a centerbody signal 7.6 cm aft of the throat is shown in figure 10. The RIAE variation was the same as in the previous case. A moderate improvement in performance from the previous case (fig. 8) is seen to occur for the larger operating point locations. This improvement results from the smaller undesirable increase in signal gain with increased airflow since the difference in inlet dynamics between the two stations is negligible (τ = 0.006 sec for both cases).

The performance with shock-wave position as a control signal is shown in figure 11. Using this signal results in good performance since it varies between the linear and optimum curves for the operating point range shown. The reason can be seen from the comparison of the steady-state shock position variation with the desired steady-state signal characteristic (fig. 6(b)). The departure from linearity for both curves is seen to be in the same direction. While the use of shock-wave position as a control signal is desirable from a performance standpoint, practical difficulties exist in its implementation. Multiple pressure locations and a means for summing them which is suitable for different flight conditions must be provided.

The effect of a control signal at an aft centerbody position in the inlet near the bypass opening is indicated in figure 12. The performance is seen to be fairly close to that of the linear case since the departure of the steady-state signal from linearity is less than that for the previous cases shown. In addition, the linear and optimum signal performances are improved from those shown previously since the time delay between the airflow near the bypass and pressure signal location no longer exists. However, the signal gain is seen to be relatively small so that the total change in static pressure over the range shown is quite small. Moreover, the generated operating point signal must be quite accurate and this accuracy must be obtained for the required range of flight conditions. Hence, while this signal is attractive from the standpoint of control of engine disturbances, serious practical difficulties, caused by the small signal variation, hinder its effective use.

Performance With On-Off Control

The performance for an example asymmetrical on-off system with the dynamics for a pressure signal near the shock wave and with the previously used controller and servo-valve dynamics is shown in figure 13. The dead zone is included so that a limit cycle will not occur in the absence of disturbances. The previously discussed RIAE constraint cannot be used for this case because the dead zone prevents the final error from approaching zero. Hence, each signal magnitude and the dead zone were selected on the basis of modified stability constraints as described in the Selection of Criterion section.

The maximum disturbance that can be controlled without inlet unstart is shown in figure 13(a), while the on-signal levels and dead zone variations are shown in figure 13(b) as functions of the modified stability constraint. The "on" signals are shown relative to the previously used normalized linear signal. For that case, the corrective signal was normalized so that a value of -1 was applied when the airflow error was at the steady-state unstart value. The ability to control disturbances which tend to unstart the inlet is somewhat improved from that obtained from the continuous signal (fig. 6(a)). However, the two cases are not strictly comparable because of the differences in stability constraint used.

To indicate the response of the on-off system to a disturbance which is different from the one used in the design criterion, the response of the system to a sinusoidal engine disturbance is shown in figure 14. For the frequency range shown, the magnitude of the input disturbance was selected so that an inlet unstart would occur for the uncontrolled case. Hence for the maximum negative curve, a unit value of (w_{c_e}/w_{c_d}) would indicate inlet unstart. Both the maximum negative and positive airflow errors are shown. While the effects of the asymmetrical signals result in a significant difference in the two error curves, the performance is felt to be good since flow errors in the more important negative direction are reduced for the entire frequency range shown. The fact that the curves do not approach unity at the high frequencies is a similar occurrence to that observed for the previous asymmetrical nonlinearities. As previously mentioned, this behavior is a consequence of the requirement that for periodic motions, the output from the nonlinearity (and resulting input to the integrating element) not contain a steady-state component.

Effects of Variations in Linear Dynamics

While the emphasis of this report has been on the influence of some of the inlet pressure signal nonlinearities on the bypass control system effectiveness, it is also of interest to vary the linear dynamics of the components relative to the inlet to give an indication of these effects. While they can, of course, be analyzed by means of established linear control theory, it is desirable to investigate them here by means of the previously used RIAE stability constraint.

Effects of varying the servo and controller frequencies (damping ratio remains constant) as well as the inlet dynamics time delay are shown in figure 15. The basic values used are the nominal ones given in the System Representation section except for the particular parameter which is varied. The steady-state relation between normal shock-wave displacement and the corrected flow change was linearized for the region near the inlet unstart condition (fig. 3). Since the controller nominal natural frequency is only slightly higher than that of the servo, the effects of their variation in terms of frequency ratio are essentially the same for the frequency range shown. However, for $(\omega_n/\omega_{n_{ref}}) \to \infty$, the maximum controllable ramp for the controller is 2 percent less than that with the servo. For both controller and servo $\omega_n \to \infty$, the maximum controllable ramp is increased by 80 percent from the nominal case.

The effects of time delay variations are also shown in figure 15. For this linear case, a time delay can occur either in the inlet, controller, or a combination of the two and have the same effect on performance. For this example, a reduction of the inlet time delay to zero represents the use of a control signal near the bypass exit. Hence, the effect of moving the control signal longitudinally from a station near the normal shock wave to the bypass station is indicated by this reduction. The reduction in time delay is seen to allow only a moderate increase in performance for the selected value of the stability constraint since the effects of the dynamics in the remaining portions of the control loop are still present.

A procedure expected to improve performance for given inlet dynamics is the addition of a lead network to compensate for the inlet and bypass dynamics together with a faster response capability for the servo and controller. The effect of modifying the controller signal with a first order lead network with a 5:1 ratio of numerator to demoninator time constants is also shown in figure 15. Nominal values of the system parameters were used. It is of interest to note that the numerator term of the lead network (0.019 sec) is somewhat greater than that which would cancel the inlet bypass time constant. A significant improvement in performance is seen when the lead network is added. However, in order to assess whether this advantage could be obtained for an actual case, some detailed knowledge of the noise characteristics of the signal pressure would be required. This additional information would then allow a more complete determination of filtering requirements. Adding the lead would, of course, also offer potential improvement for the previously discussed on-off case as well as for the previously discussed nonlinear signals.

Effect of Example Gust Disturbance

Although not intended to be used for selecting control system parameters, the controlled inlet response to an external disturbance was also investigated for the linear case. It may be noted that higher performance in the control of external disturbances may potentially be obtained with a more forward control of the inlet flow, such as a throat area control, and with a forward control signal location. However, as previously mentioned, using only a single high performance control system (the bypass control) is desirable if the resulting performance for expected external disturbances is at least adequate. The constants for the previously described nominal linear bypass control system, with the control signal located slightly aft of the inlet throat, were used. The transfer function for the response of this controlled system in terms of shock-wave displacement due to an external disturbance expressed as a shock-wave displacement was determined. The external disturbance used was a statistically described longitudinal gust which was assumed to be only a velocity disturbance. The constants representing the gust power spectrum and the transfer function relating a longitudinal velocity disturbance to the inlet shock-wave position were given in the System Representation section. The full-scale gust frequencies were increased by a factor of 3 to be compatible with the dynamics of the one-third scale model. The resulting power spectra of shock-wave position with and without the control system are shown in figure 16. Shock-wave position is used as the output parameter to indicate

the tendency toward inlet unstart due to the disturbance. The results indicate the response of the shock-wave position of the one-third scale model to atmospheric gusts with an rms magnitude of 1 mps. The resulting rms shock-wave excursion of the model will be proportional to an estimate of the rms gust magnitude.

An examination of figure 16 indicates a moderate improvement in rms shock-wave excursion for the controlled case over the uncontrolled case. While the response for the low frequency range is improved, the disturbance to the inlet still has significant power for a frequency range above that for which the control system is effective. As was mentioned for the engine disturbance case, signal lead and higher frequency system components would improve the control system response at the higher frequencies. However, possible effects of signal noise would need to be investigated in order to obtain realistic performance estimates.

An estimate of the tendency toward inlet unstart for a selected inlet operating point flow condition and for an estimated rms gust velocity can be obtained as was described in the System Representation section. While present measured gust data for the high cruise altitudes of interest are rather limited, some preliminary results have been reported (ref. 9). As a numerical example, a fairly high rms turbulence level for a supersonic transport cruise altitude of 3.05 mps was selected. The resulting rms shock-wave variations of 0.43 cm for the controlled case and 0.49 cm for the uncontrolled case are obtained from figure 16. A representative operating point to allow a margin for control of internal disturbances was selected to be 2.3 cm (1.65 percent supercritical airflow). This value is seen to be relatively large in comparison to the calculated rms shock-wave excursions. The corresponding average unstarts per hour, N, were calculated from the values of N_o given in figure 16 and the equation in the External Disturbance section. The resulting values are 0.087 unstarts per hour for the controlled case and 2.1 unstarts per hour for the uncontrolled case for the assumed high rms level of turbulence of 3.05 mps. Note that these unstart rates are in terms of model dynamics, so that for a full-scale inlet, they would be reduced by a factor of 3. The control is seen to be effective in terms of the unstart frequency parameter. For this example, the inlet unstart frequency is seen to be quite small for both cases for the turbulence level and inlet flow operating point assumed. However, as previously mentioned, values used for the transfer function between the atmospheric gust and shock-wave excursion and estimates of the gust structure were rather preliminary, and, hence, further work is needed to assess the importance of atmospheric gust disturbances on inlet operation.

CONCLUDING REMARKS

Some of the closed-loop control aspects of an inlet bypass system have been investigated. While the computed results were presented only for a particular inlet, parameters and a performance criterion were selected which should facilitate comparisons of bypass control performance with other inlets.

The criterion consisted of the maximum engine disturbance rate which could be controlled subject to a time domain stability constraint. The constraint was relaxed for initial errors in the decreased airflow direction for which the inlet tends to unstart. The change improved the ability to correct the larger errors in this direction while maintaining the desired stability near the operating point. For given inlet and control system component dynamics, the desired nonlinear signal variation to achieve this result was obtained. This signal shape was closely approximated by a parabolic variation in the decreased airflow direction and a linear variation in the opposite direction and can be used as an aid in selecting available pressure signals. The effects on control-system performance of measured nonlinear signal characteristics at several locations were evaluated. Although from the performance standpoint, control was most effective with a pressure signal located near the bypass opening, performance with the more forward locations was also of interest because of the higher pressure-signal gain available. The difference in linear dynamics when the signal was located forward of rather than near the bypass opening tended to degrade the performance. However, an even more adverse effect was due to the more nonlinear variations for the more forward locations. One means for avoiding this adverse effect would be to add an additional pressure signal so that the summed signal would have an acceptable variation. A simplified form of this addition was investigated, in which only an on-off signal was added, and shown to give satisfactory results.

The performance of a system with an asymmetrical on-off control was determined. This system was shown to be as good as the nonlinear continuous-control system for disturbances that tended to unstart the inlet, although somewhat greater errors would occur as a result of disturbances in the opposite direction. This form of control would offer potential simplifications in the sensing and computing elements of the system.

Ames Research Center
National Aeronautics and Space Adminstration
Moffett Field, Calif., 94035, March 20, 1967
720-03-01-01-00-21

REFERENCES

1. Lockheed-California Co.: Investigation of Supersonic Transport Engine Inlet Configurations. NASA CR-68399, 1965.

2. Chun, K. S.; and Swanson, D. B.: Dynamic Simulation of Supersonic Inlet and Engine. AIAA Paper 64-598, 1964.

3. Flanders, T. A.: Control of Supersonic Inlets. ASME Paper 61-AV-65, 1961.

4. Kepler, C. Edward; and Barry, Frank W.: Engine Air Inlet Compatibility for the Supersonic Transport. SAE Paper 650225, 1965.

5. Barry, Frank W.: Effects of Atmospheric Gust Criteria on Supersonic Inlet Performance. AMS/AIAA Paper 66-367, 1966.

6. Bowditch, David N.; and Wilcox, Fred A.: Dynamic Response of a Supersonic Diffuser to Bypass and Spike Oscillation. NASA TM X-10, 1959.

7. Houbolt, John C.; Steiner, Roy; and Pratt, Kermit G.: Dynamic Response of Airplanes to Atmospheric Turbulence Including Flight Data on Input and Response. NASA TR R-199, 1964.

8. Rhyne, R. H.; and Steiner, R.: Power Spectral Measurement of Atmospheric Turbulence in Severe Storms and Cumulus Clouds. NASA TN D-2469, 1964.

9. Crooks, Walter M.: High Altitude Clear Air Turbulence. AFFDL-TR-65-144, 1965.

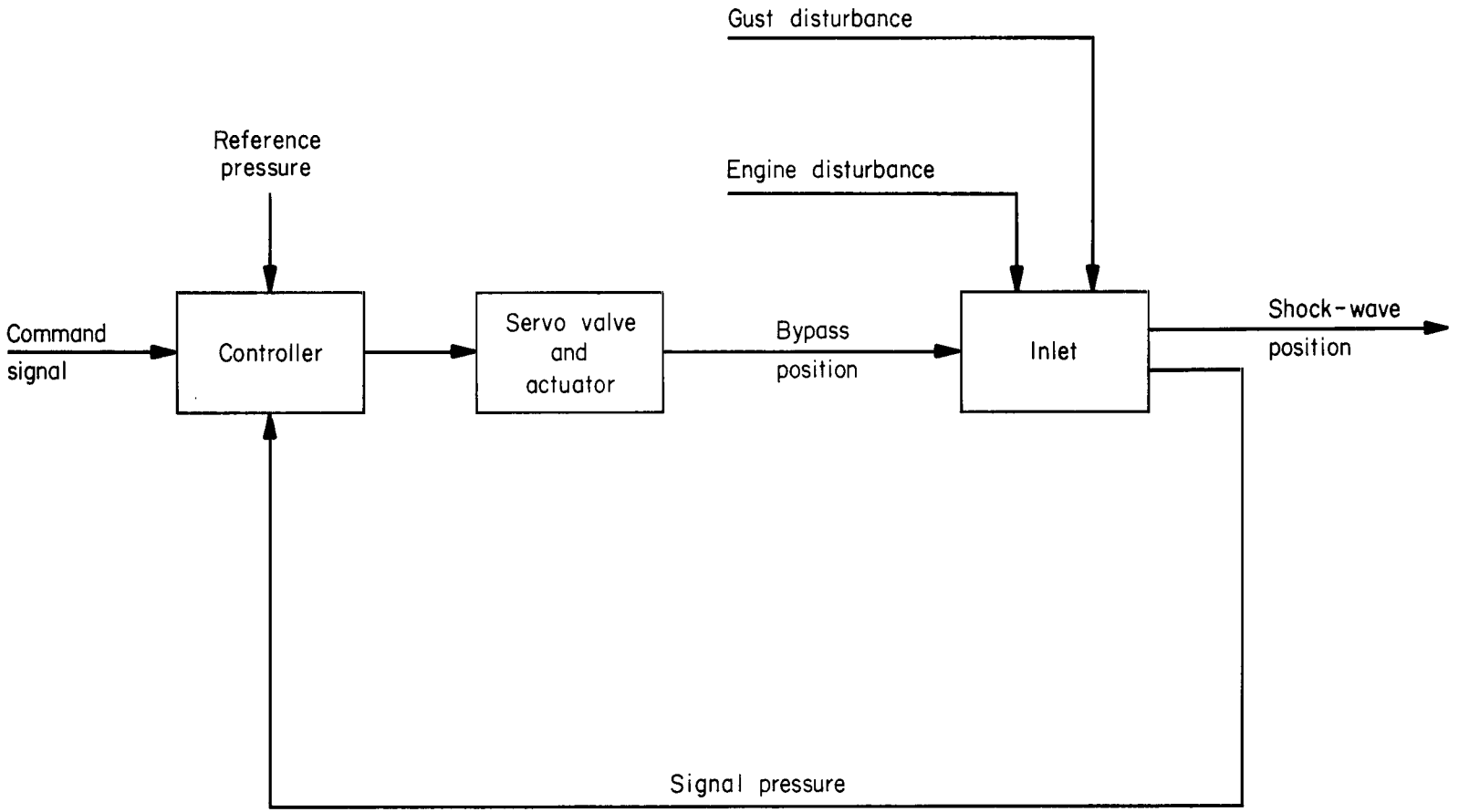

Figure 1.- Block diagram of inlet bypass control system.

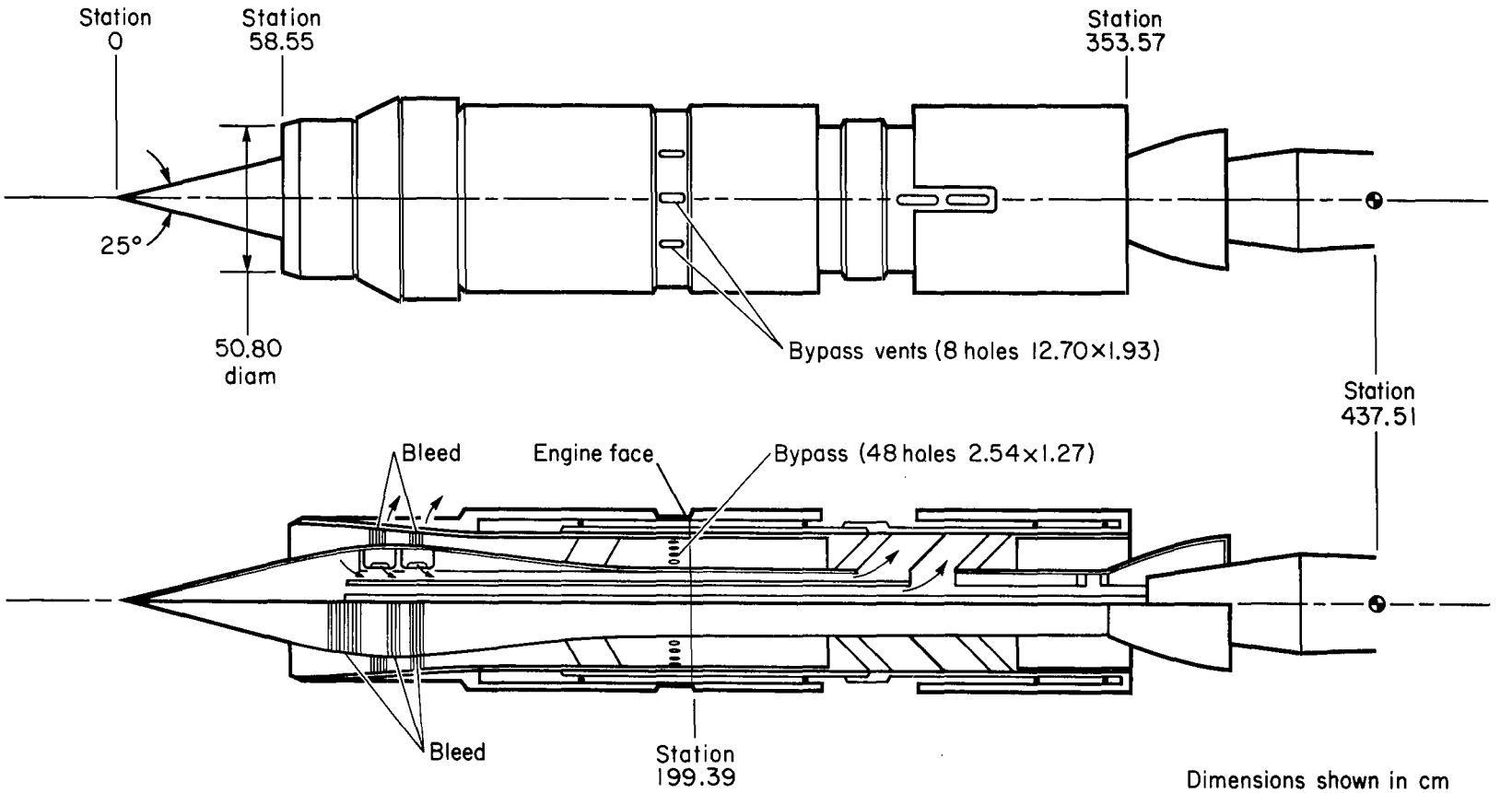

(a) Wind-tunnel model

Figure 2.- Example inlet configuration.

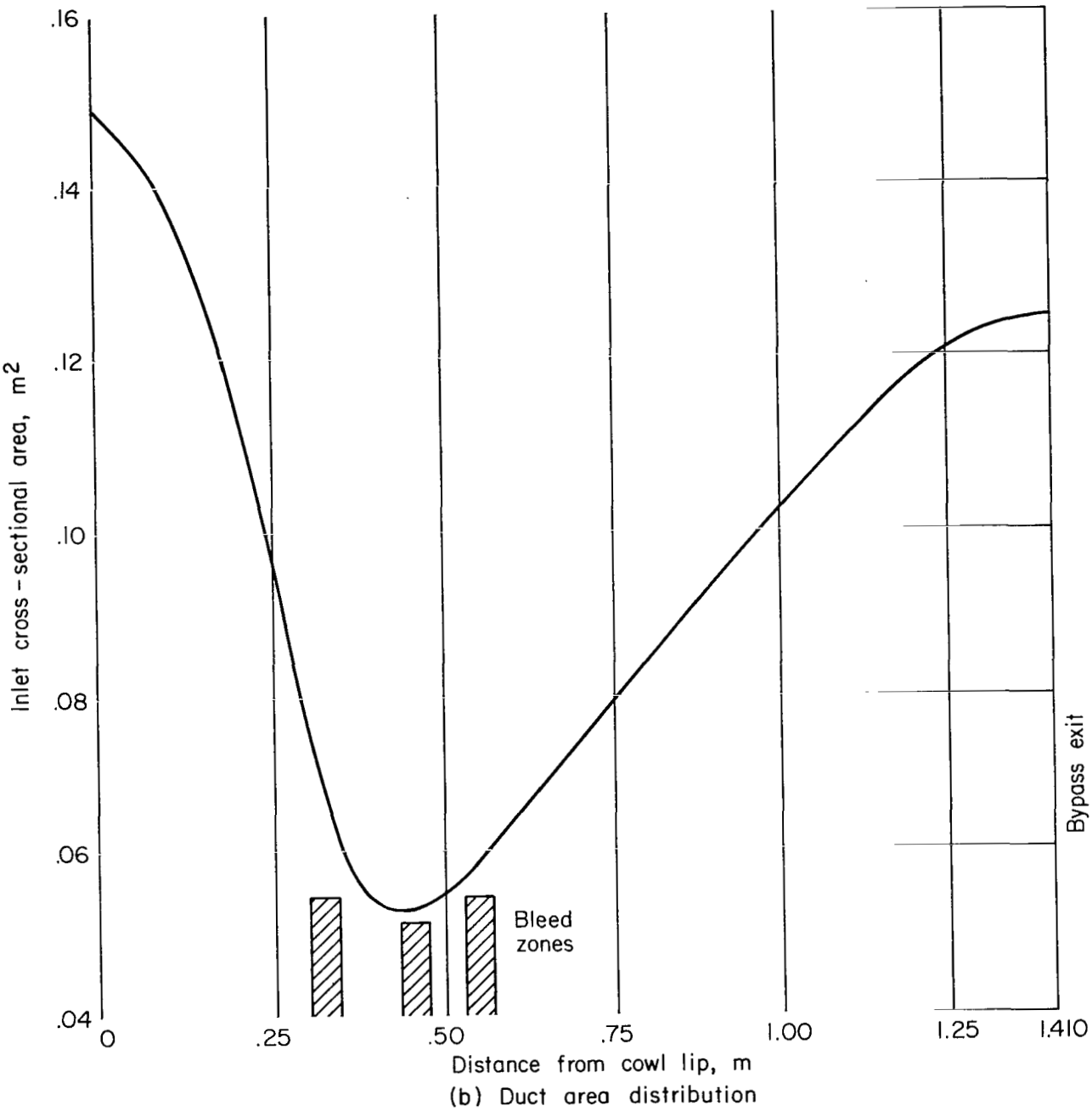

(b) Duct area distribution

Figure 2.- Concluded.

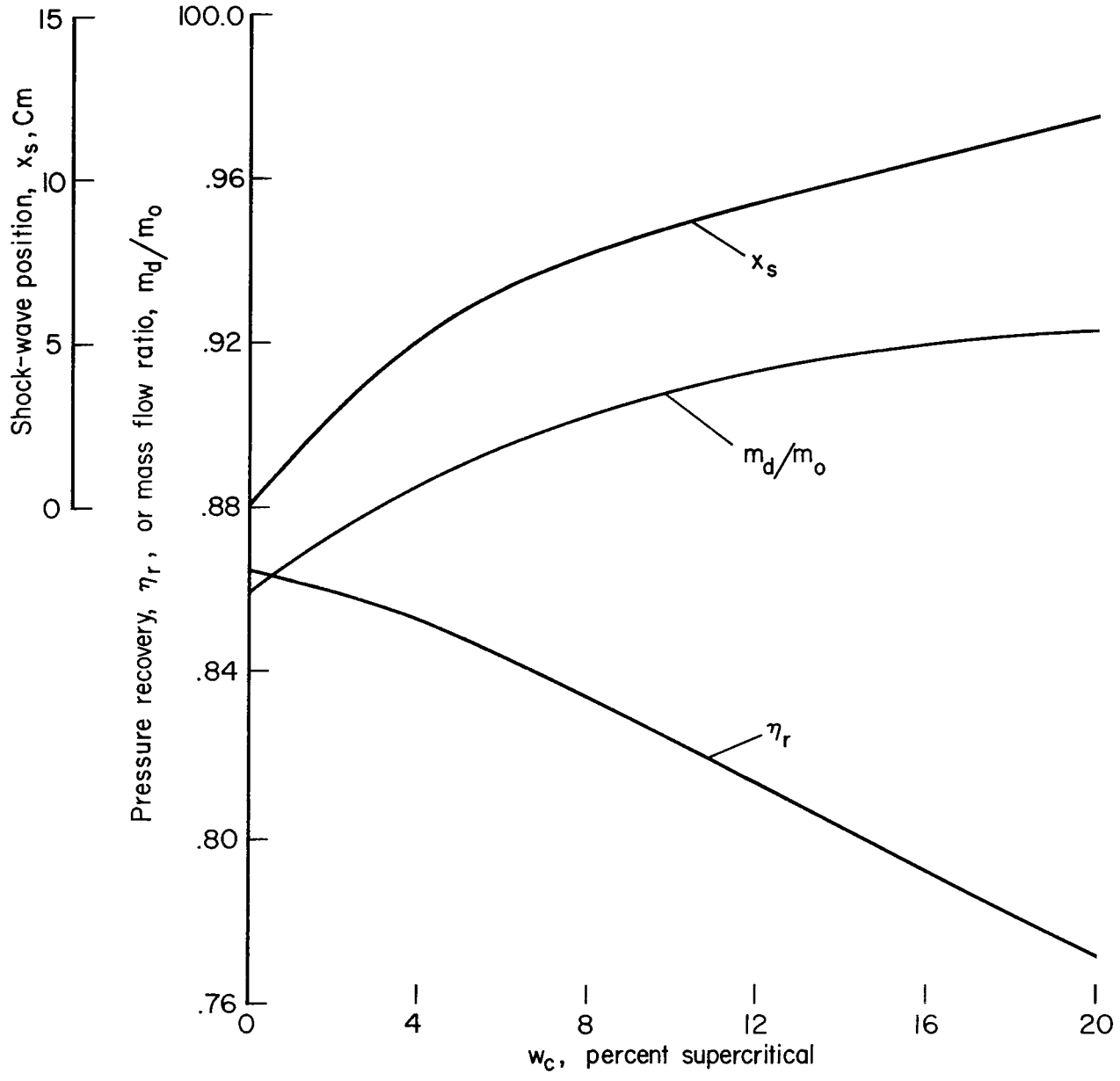

Figure 3.- Steady-state characteristics of example inlet; $M_\infty = 3.0$

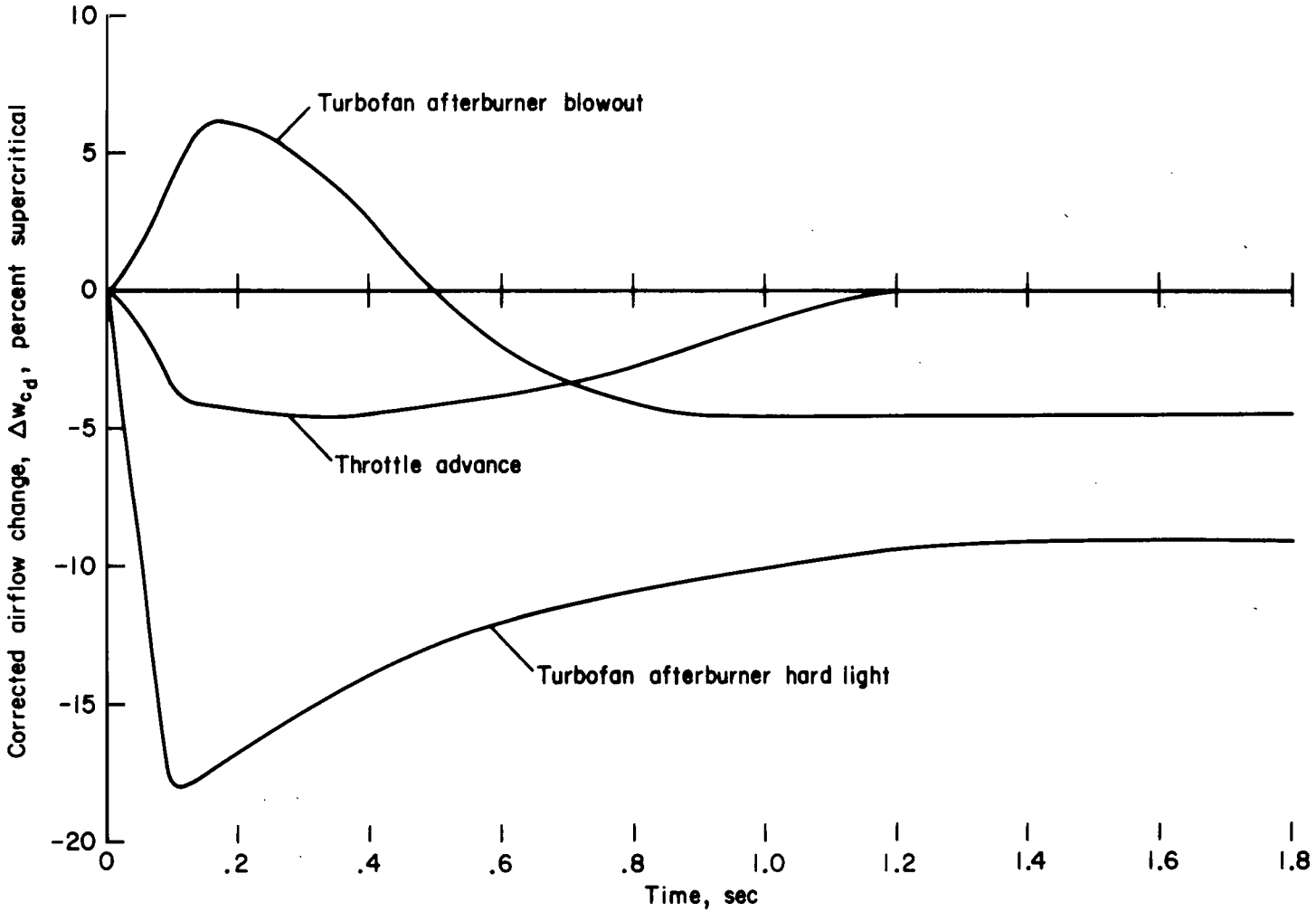

Figure 4.- Typical engine disturbances to the one-third scale model inlet.

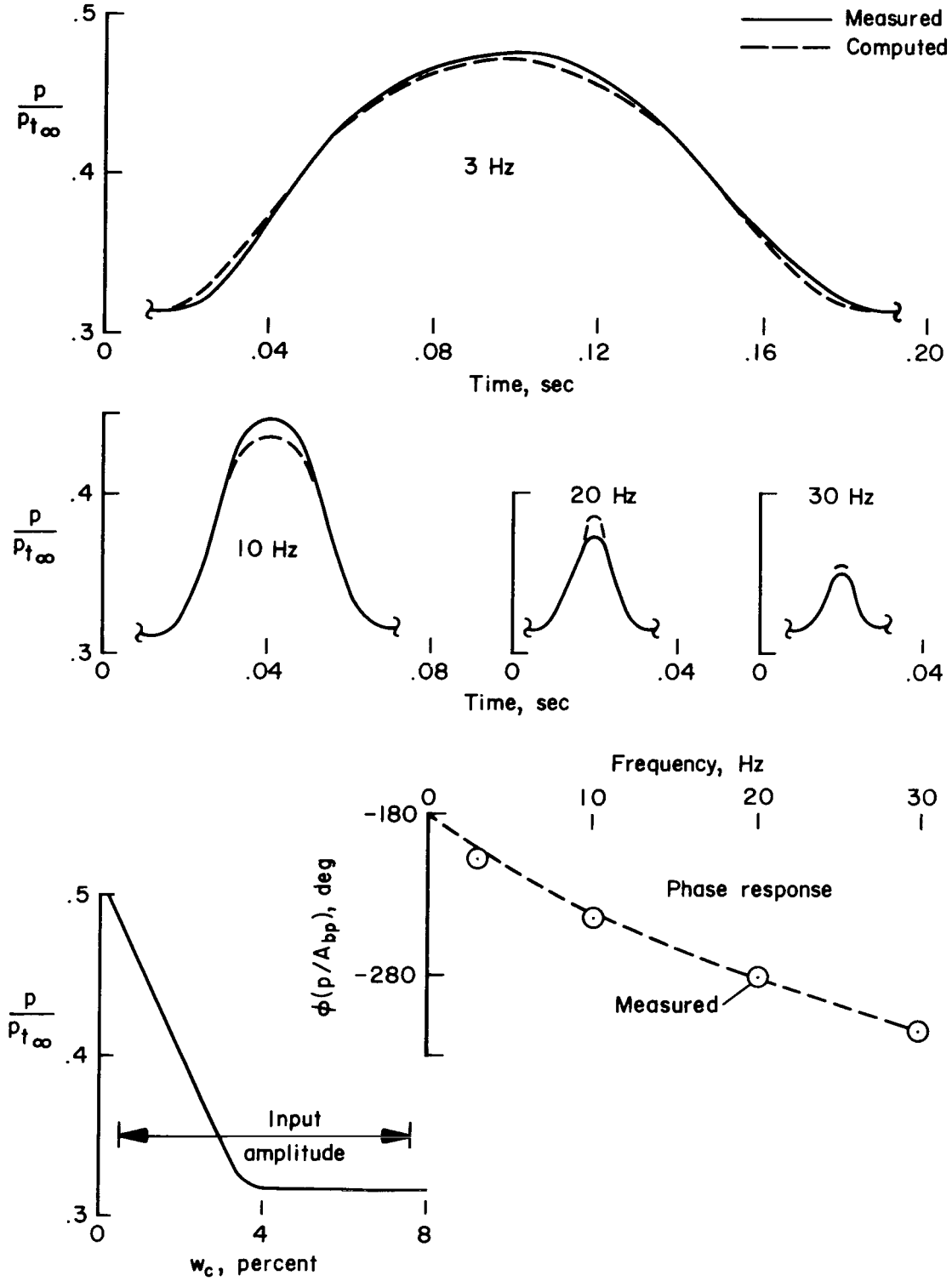

Figure 5.- Comparison of measured and computed pressure characteristics at a center-body station 1.3 cm downstream of the geometric throat resulting from a sinusoidal bypass disturbance.

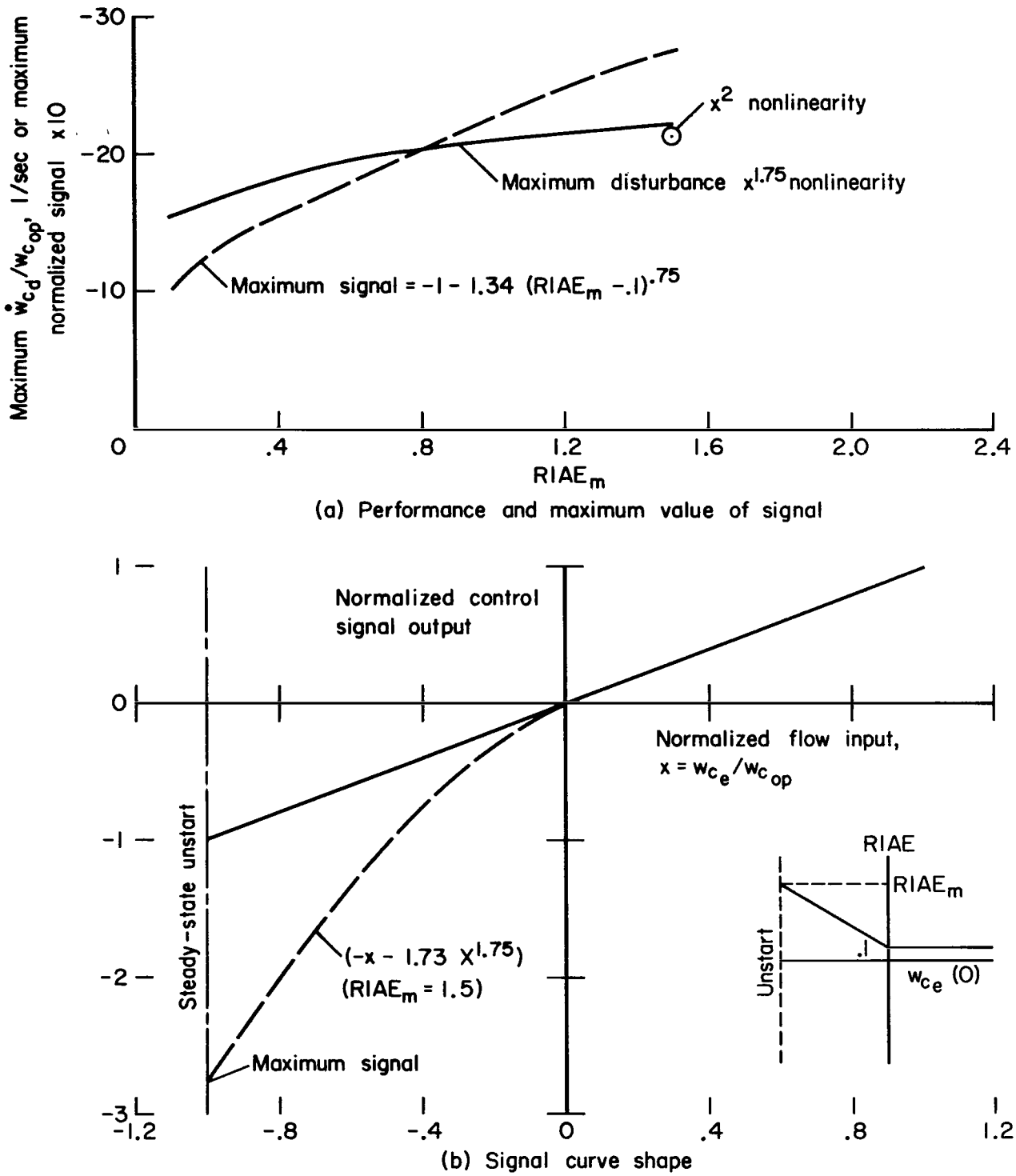

Figure 6.- Effect of variations in RIAE constraint for a control signal near the shock-wave position.

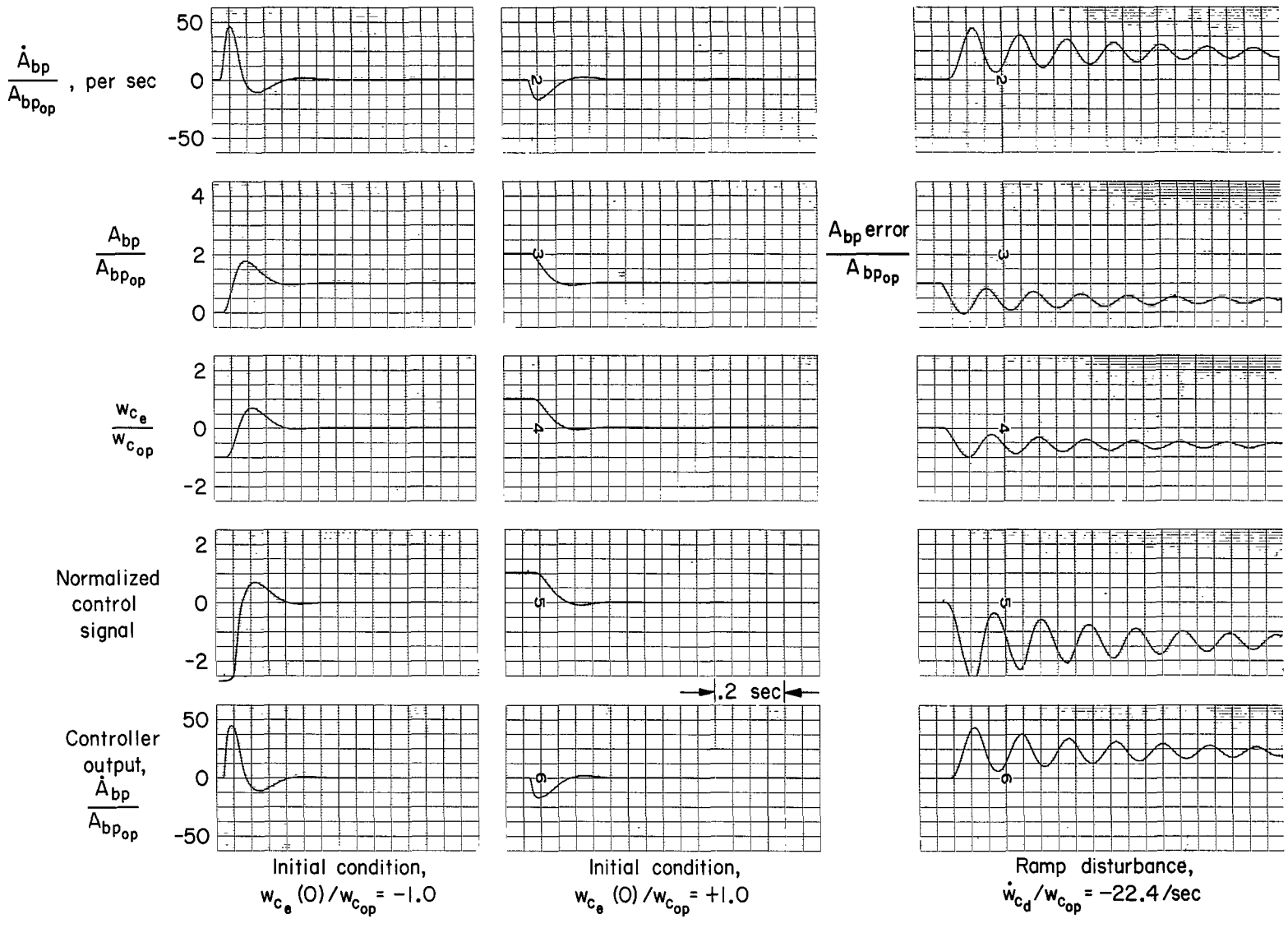

(c) Example time histories with optimal signal shape, $RIAE_m = 1.5$

Figure 6.- Concluded.

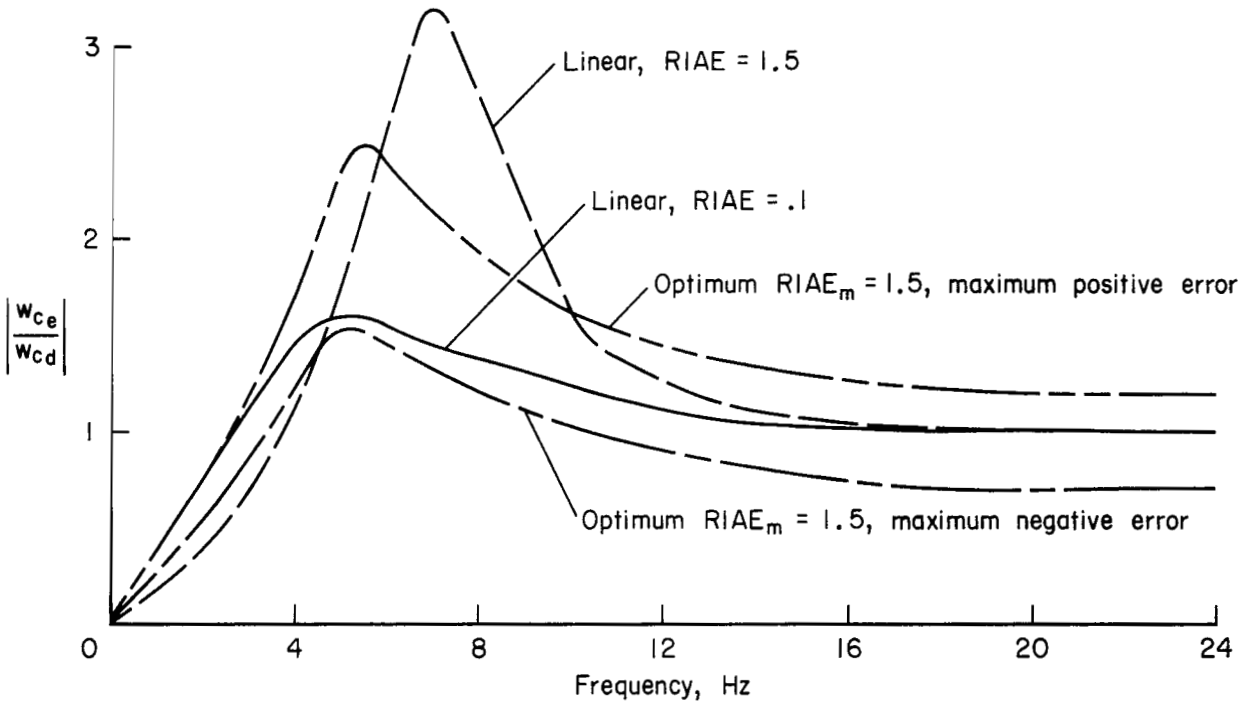

Figure 7.- Response of closed-loop systems with nonlinear optimum and linear signals to a sinusoidal disturbance.

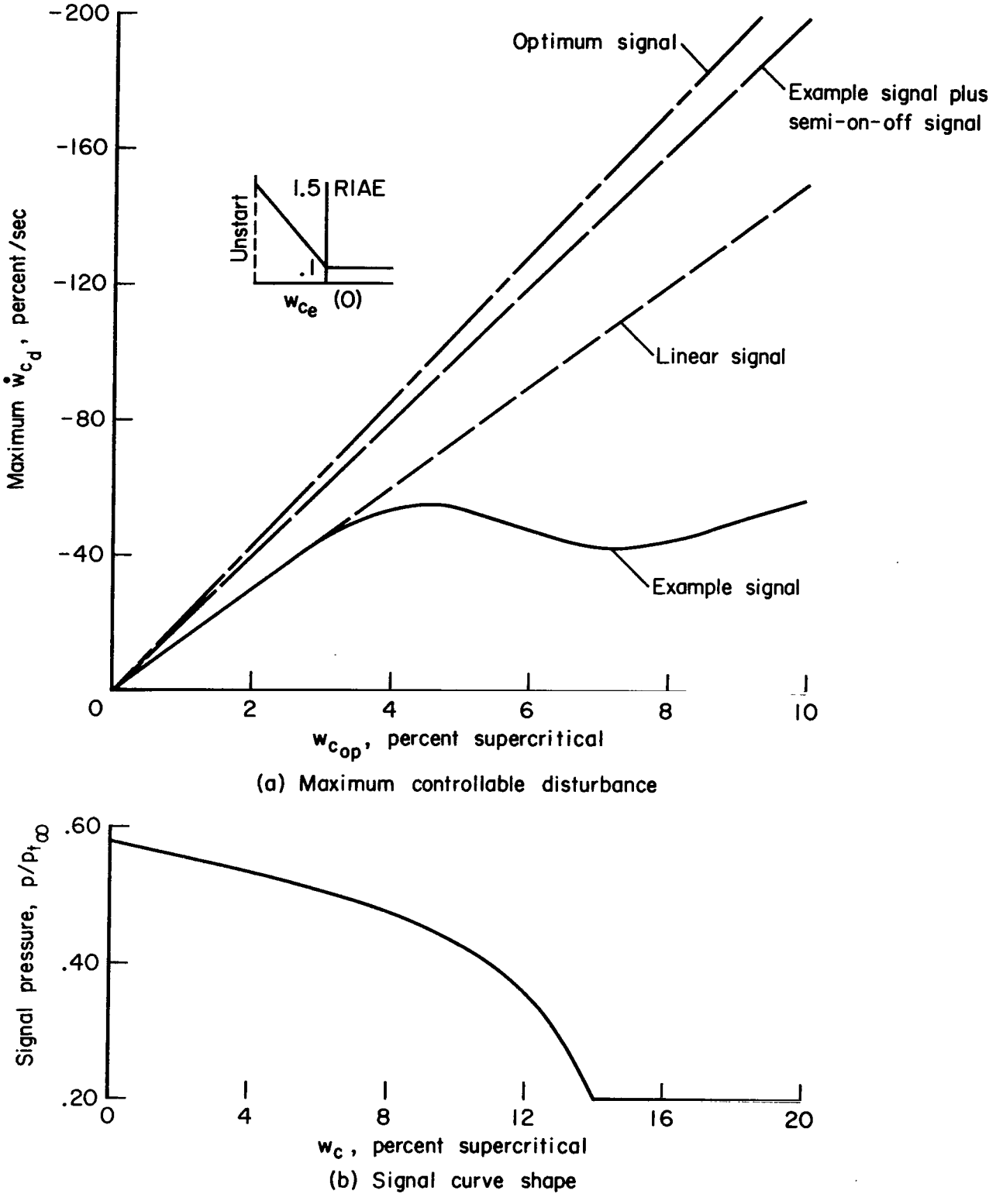

Figure 8.- Performance with control signal located 3.1 cm aft of geometric throat.

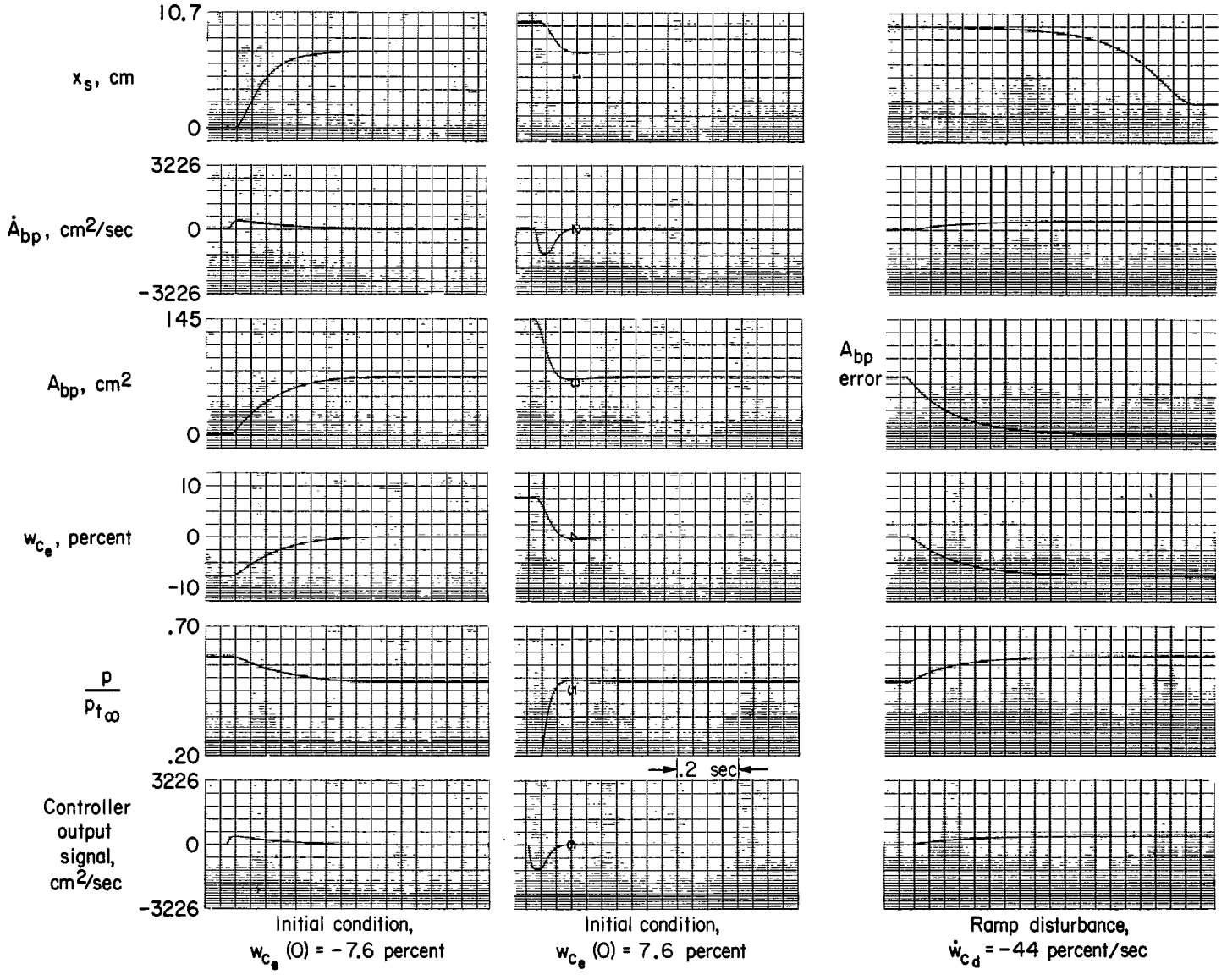

(c) Typical time histories, $w_{c_{op}} = 7.67$

Figure 8.- Concluded.

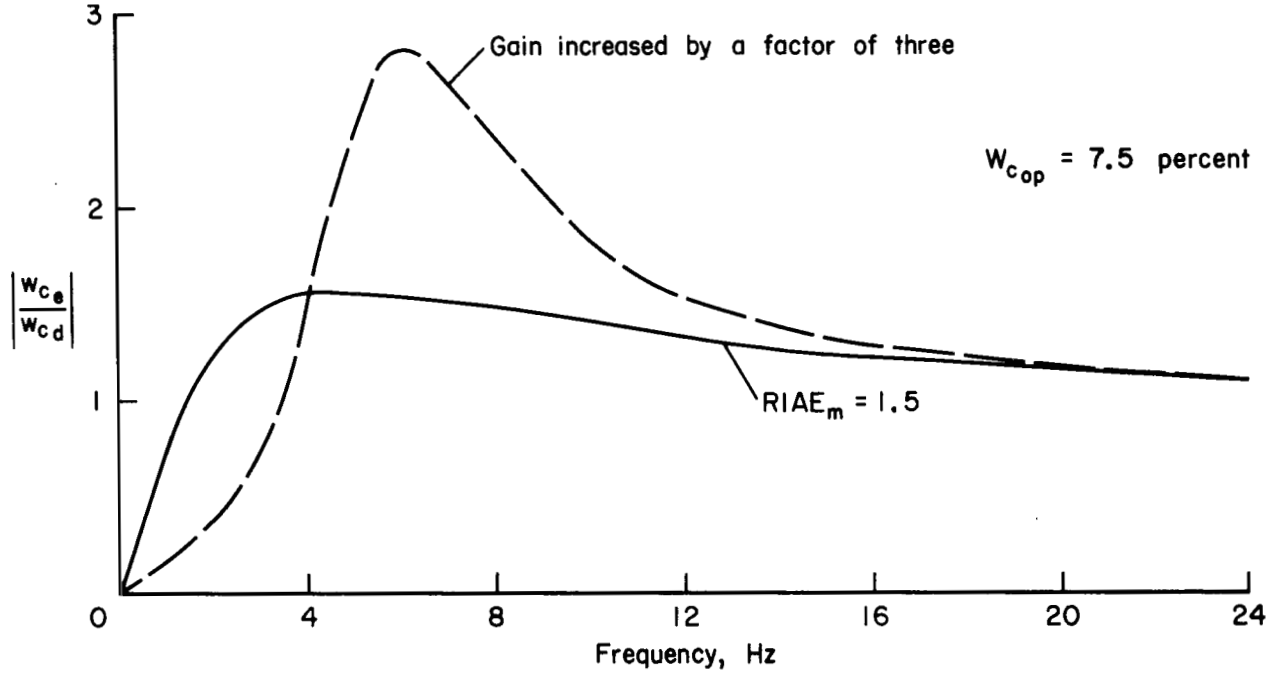

Figure 9.- Maximum negative error of system with a signal 3.1 cm aft of geometric throat due to a sinusoidal disturbance.

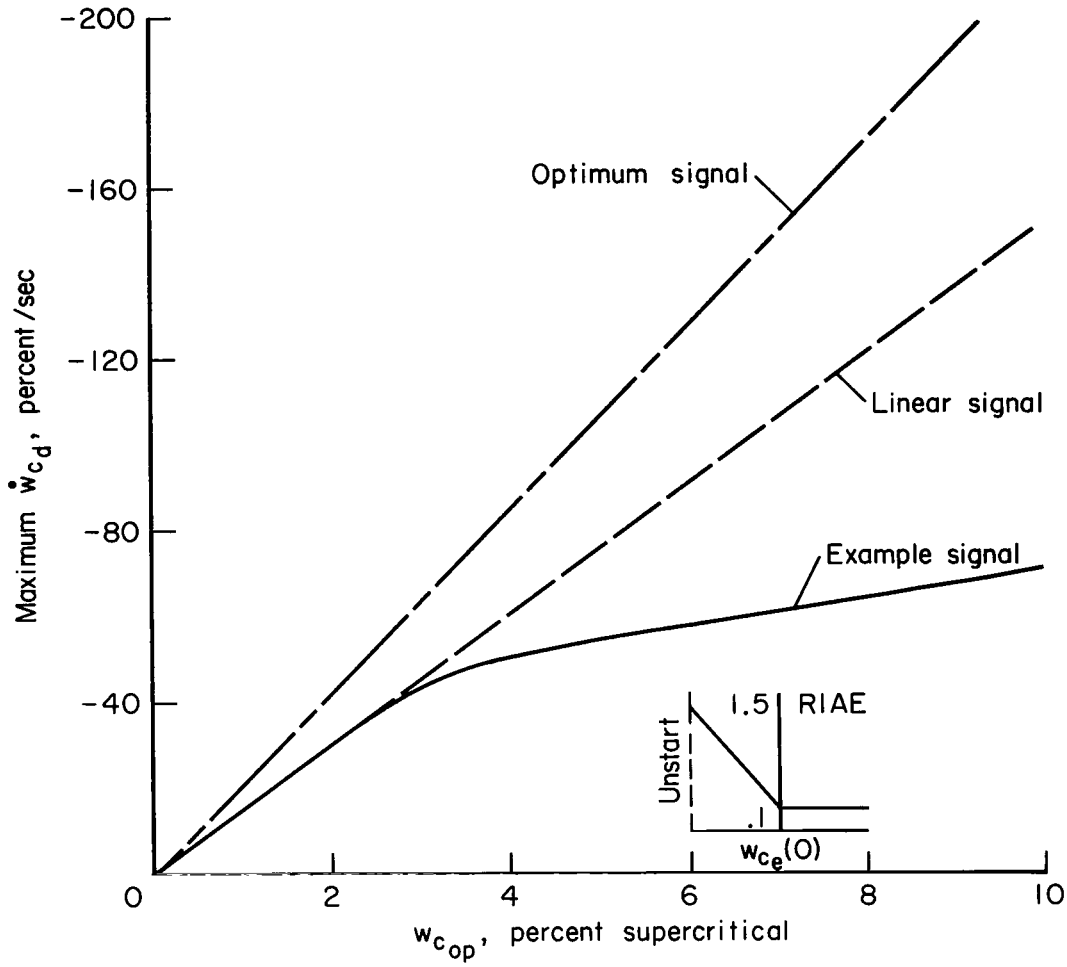

(a) Maximum controllable disturbance

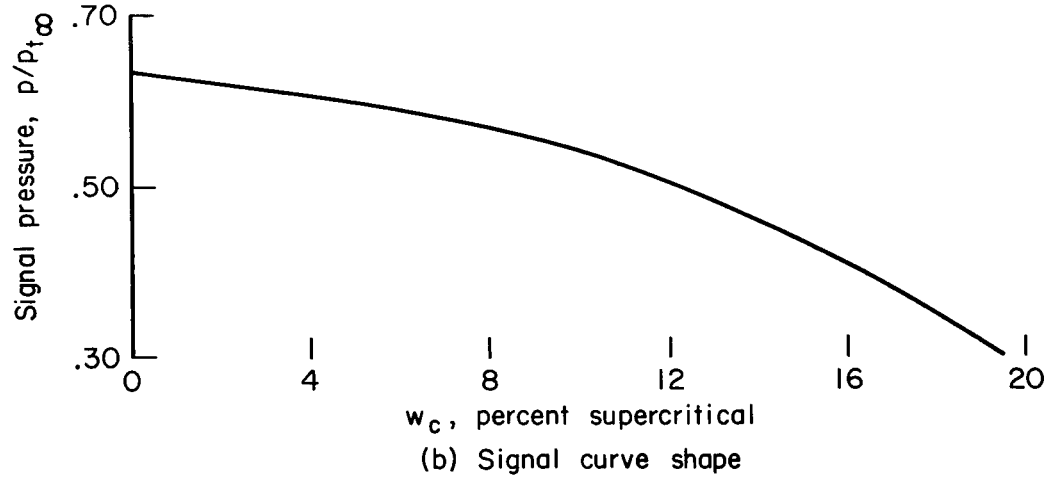

(b) Signal curve shape

Figure 10.- Performance with control signal located 7.6 cm aft of geometric throat.

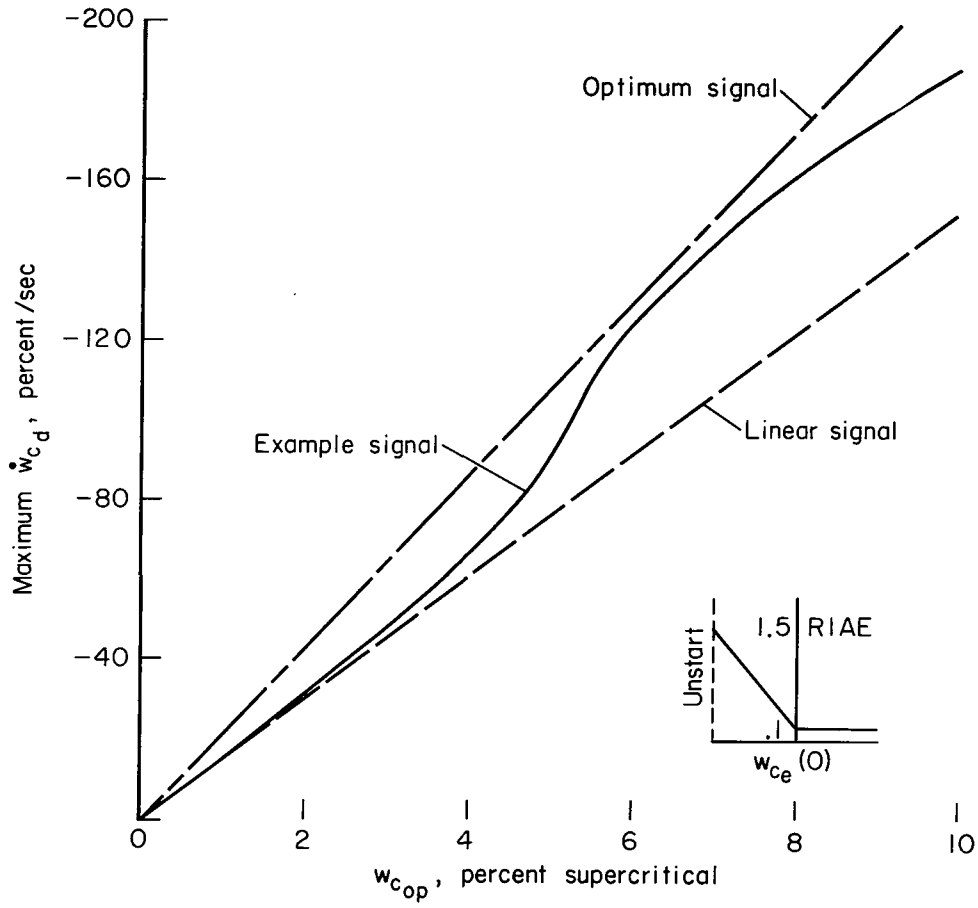

(a) Maximum controllable disturbance

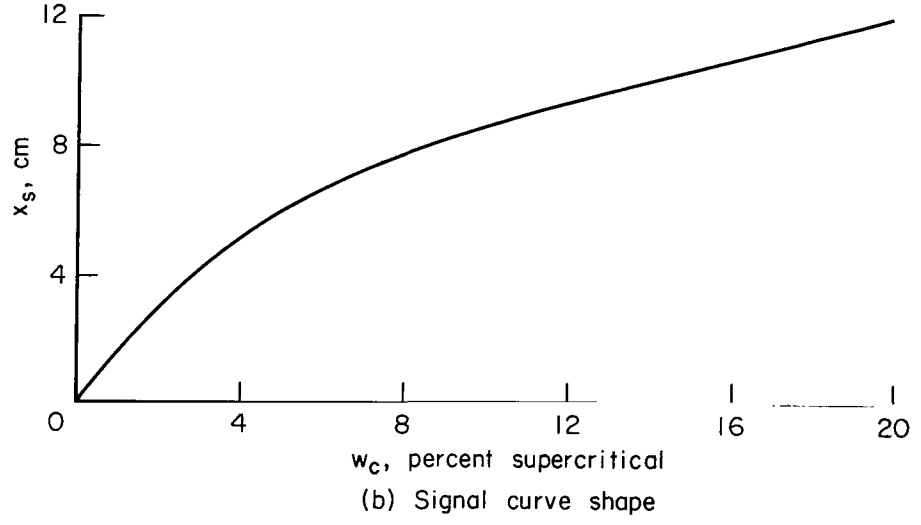

(b) Signal curve shape

Figure 11.- Performance with shock-wave position as a control signal.

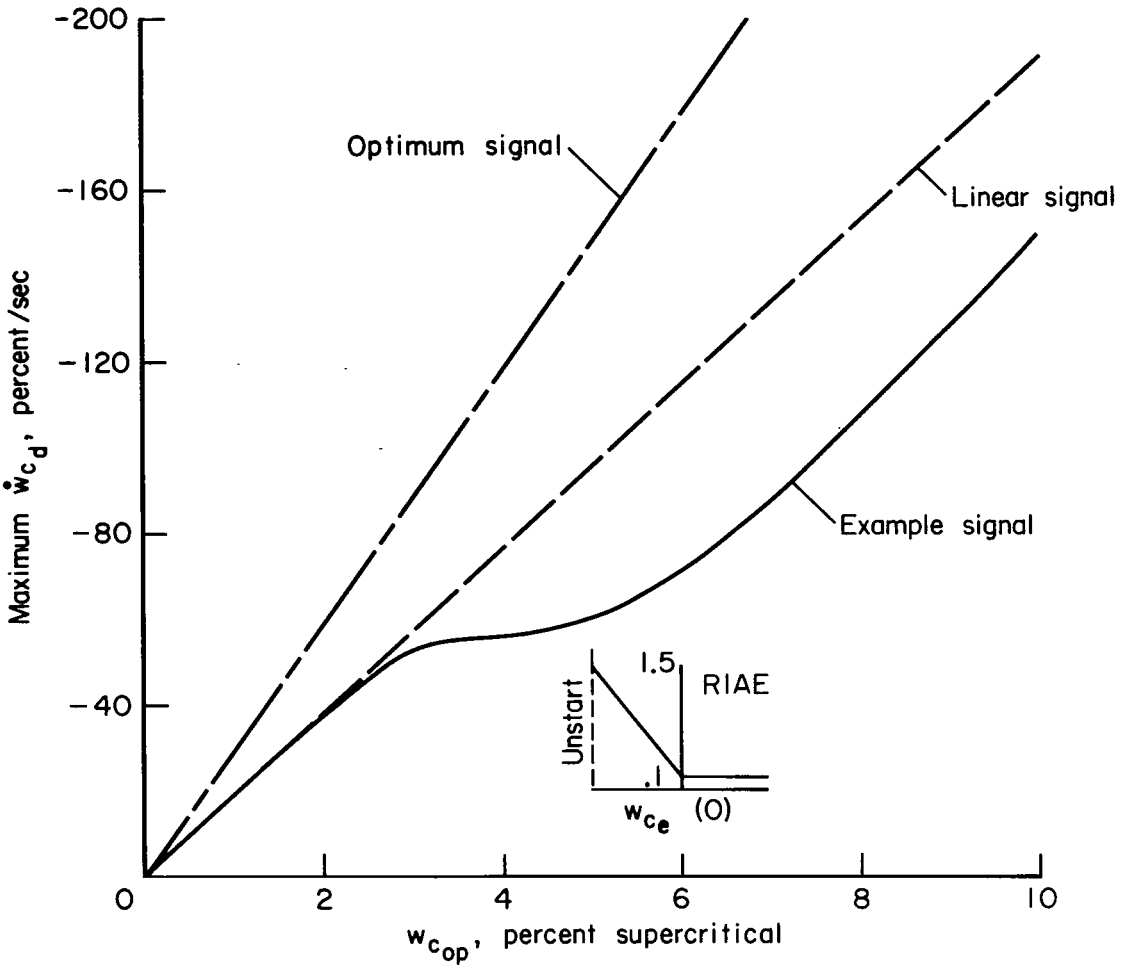

(a) Maximum controllable disturbance

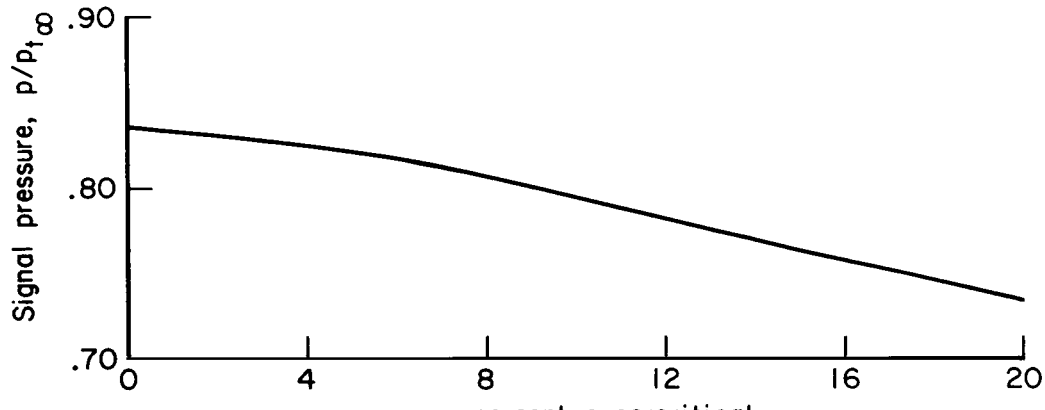

(b) Signal curve shape

Figure 12.- Performance with control signal located near bypass opening.

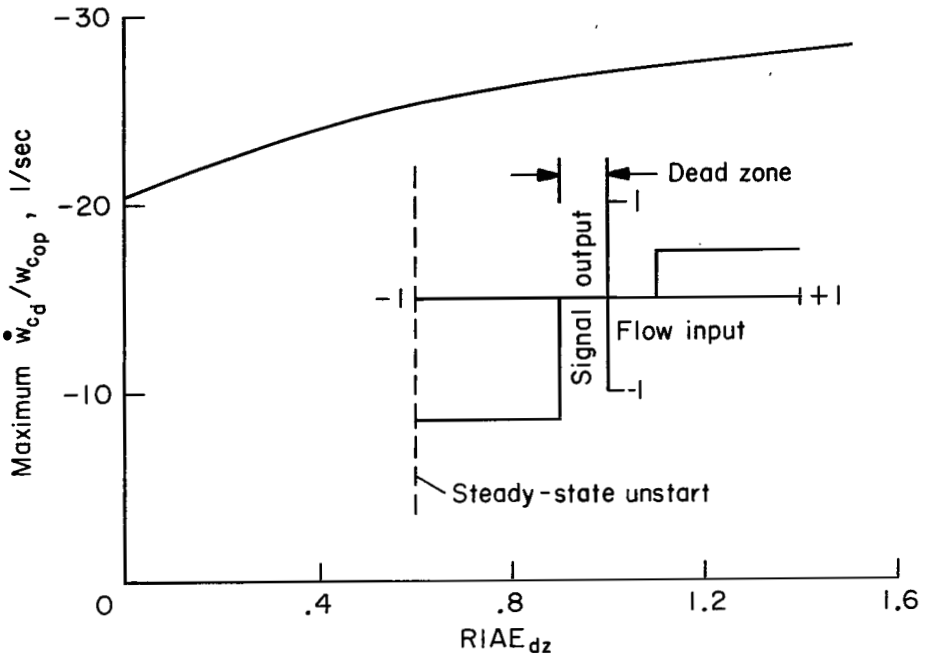

(a) Maximum controllable disturbance

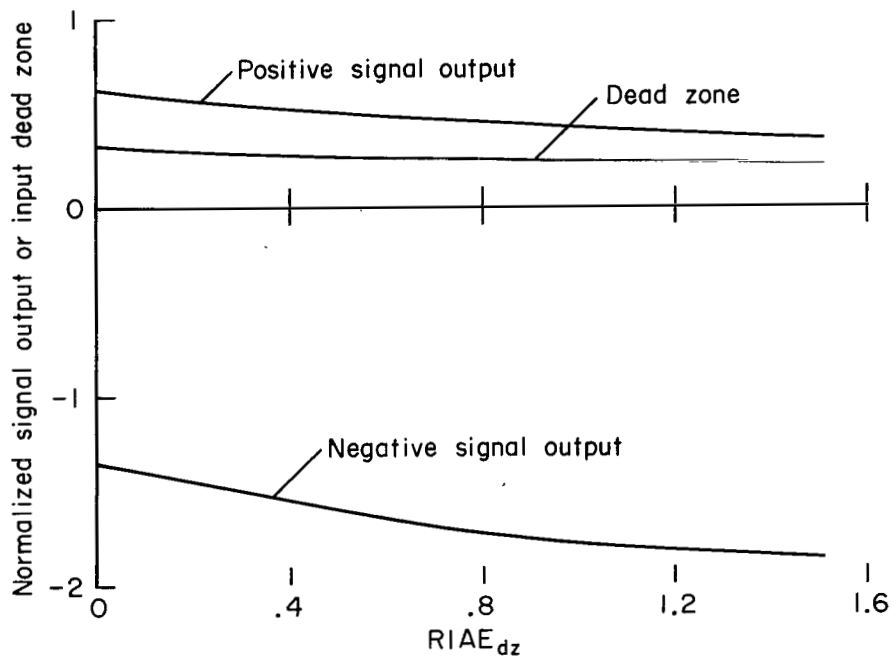

(b) Signal curve shape

Figure 13.- Performance of on-off system with control signal near the shock-wave position.

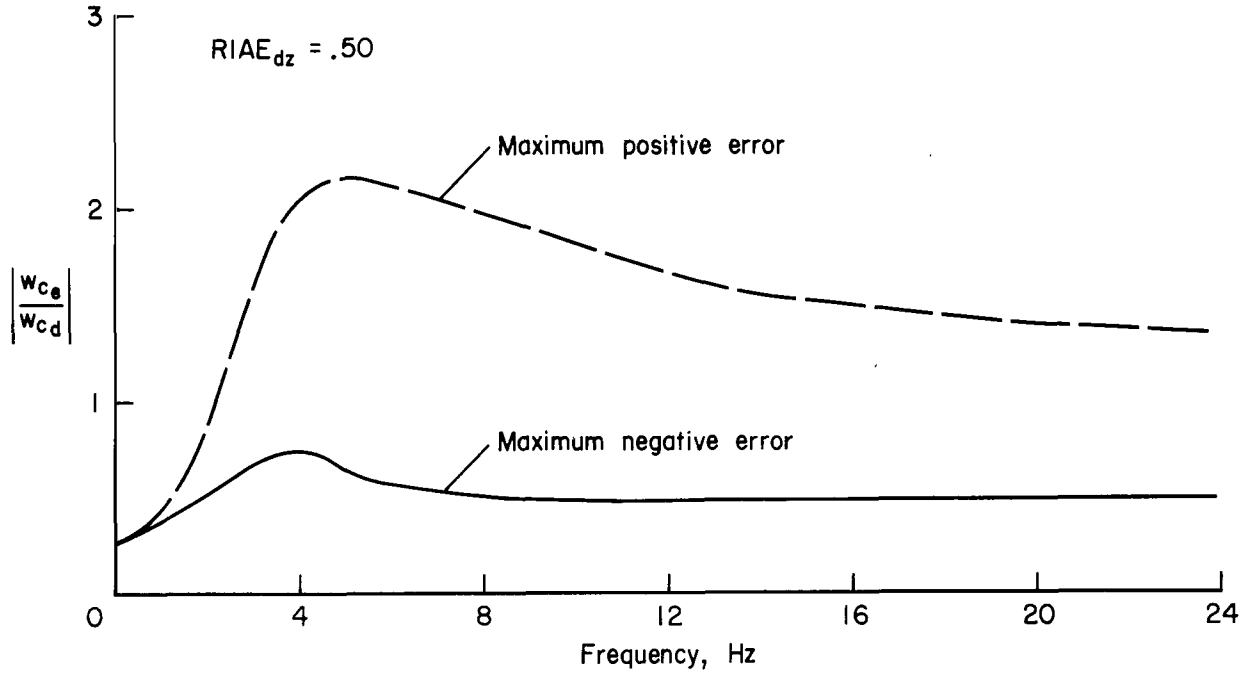

Figure 14.- Response of closed-loop system with an on-off signal to a sinusoidal disturbance.

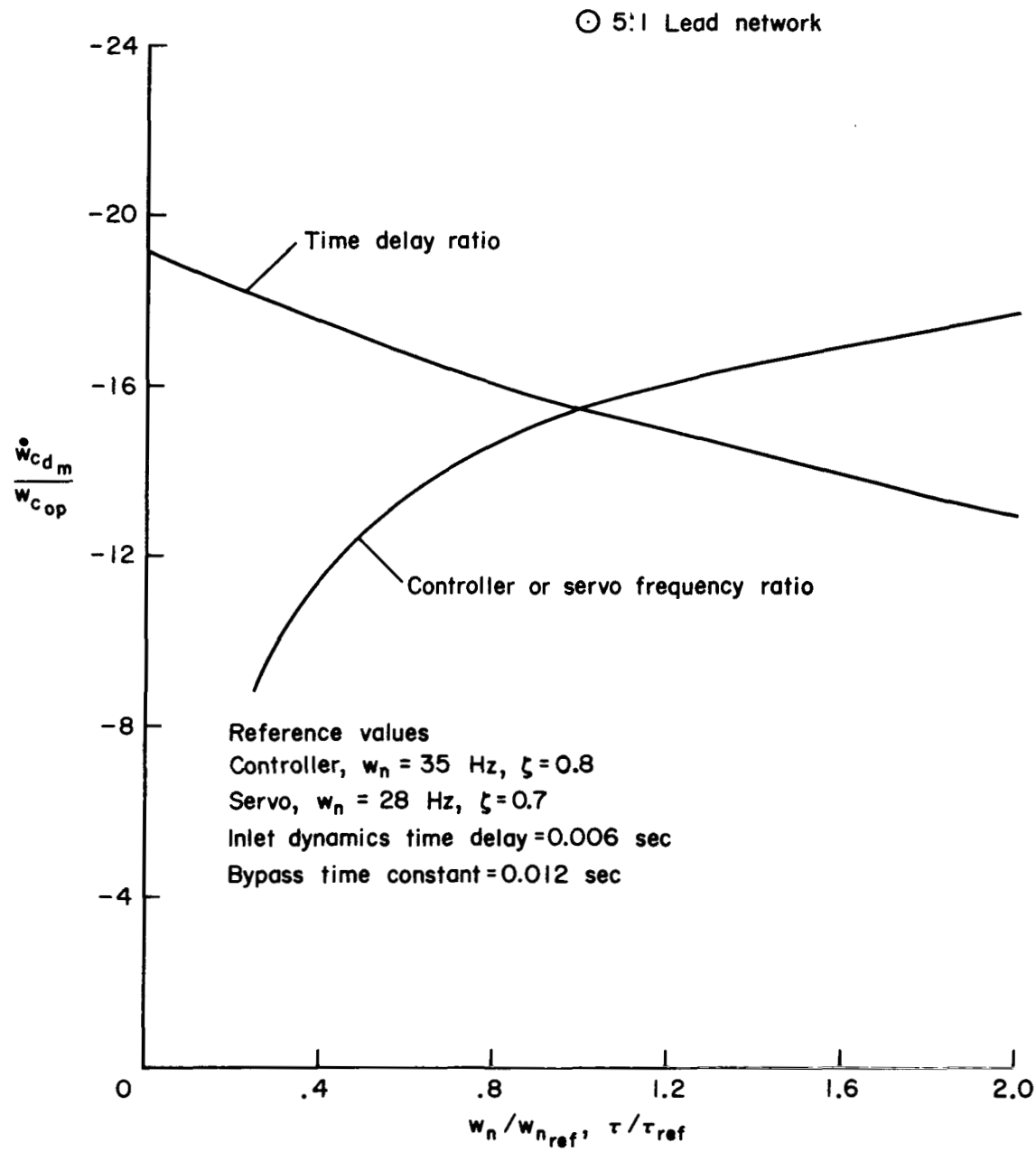

Figure 15.- Effect of servo and controller frequencies, system time delay, and lead network on performance for linear case; RIAE = 0.1.

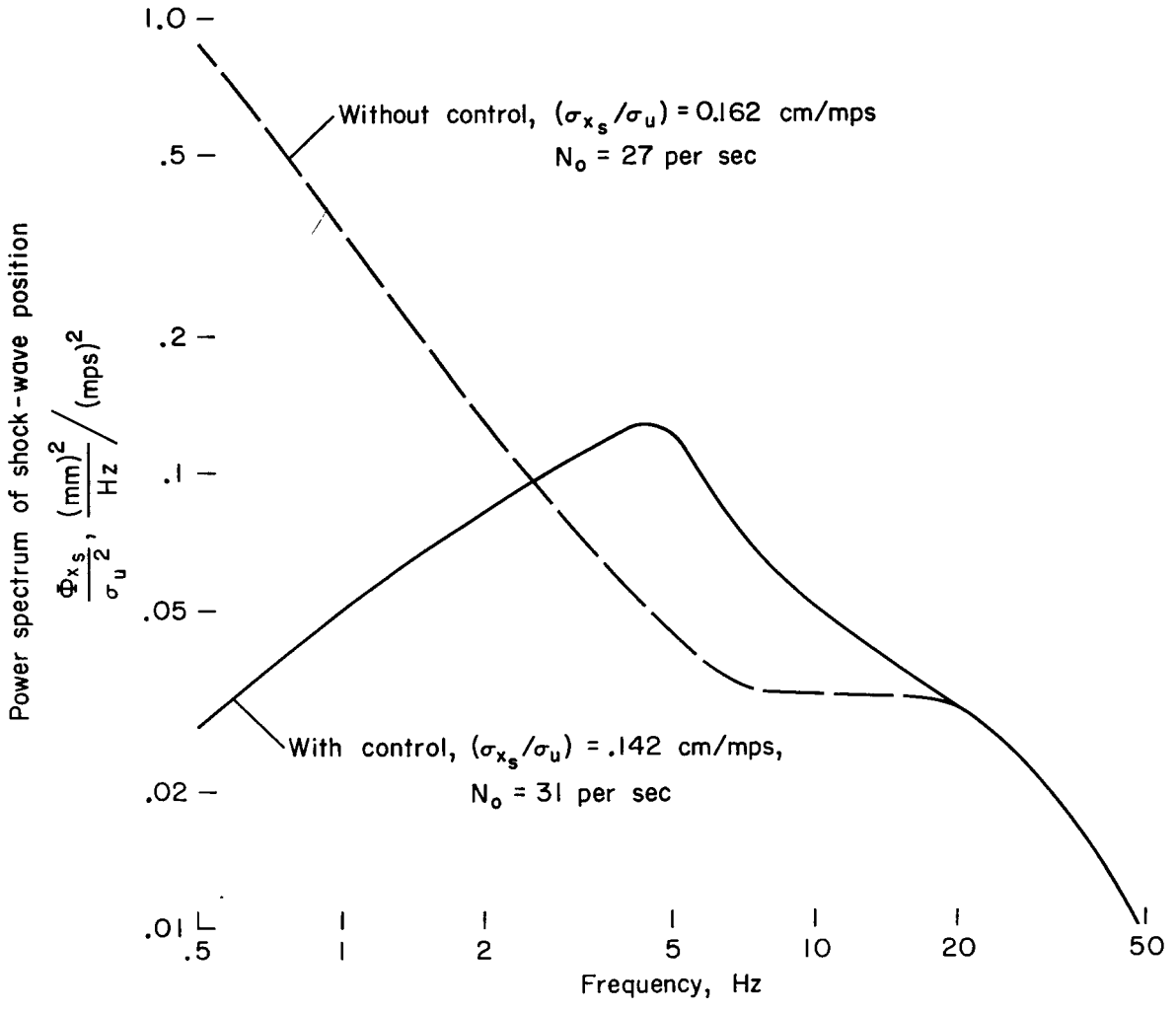

Figure 16.- Power spectra of shock-wave excursion due to longitudinal gust.

"The aeronautical and space activities of the United States shall be conducted so as to contribute . . . to the expansion of human knowledge of phenomena in the atmosphere and space. The Administration shall provide for the widest practicable and appropriate dissemination of information concerning its activities and the results thereof."

—NATIONAL AERONAUTICS AND SPACE ACT OF 1958

NASA SCIENTIFIC AND TECHNICAL PUBLICATIONS

TECHNICAL REPORTS: Scientific and technical information considered important, complete, and a lasting contribution to existing knowledge.

TECHNICAL NOTES: Information less broad in scope but nevertheless of importance as a contribution to existing knowledge.

TECHNICAL MEMORANDUMS: Information receiving limited distribution because of preliminary data, security classification, or other reasons.

CONTRACTOR REPORTS: Scientific and technical information generated under a NASA contract or grant and considered an important contribution to existing knowledge.

TECHNICAL TRANSLATIONS: Information published in a foreign language considered to merit NASA distribution in English.

SPECIAL PUBLICATIONS: Information derived from or of value to NASA activities. Publications include conference proceedings, monographs, data compilations, handbooks, sourcebooks, and special bibliographies.

TECHNOLOGY UTILIZATION PUBLICATIONS: Information on technology used by NASA that may be of particular interest in commercial and other non-aerospace applications. Publications include Tech Briefs, Technology Utilization Reports and Notes, and Technology Surveys.

Details on the availability of these publications may be obtained from:

SCIENTIFIC AND TECHNICAL INFORMATION DIVISION

NATIONAL AERONAUTICS AND SPACE ADMINISTRATION

Washington, D.C. 20546